

*Extratropical transition of tropical cyclones  
in a multiresolution ensemble of  
atmosphere-only and fully coupled global  
climate models*

Article

Accepted Version

Baker, A. J. ORCID: <https://orcid.org/0000-0003-2697-1350>,  
Roberts, M. J., Vidale, P. L. ORCID: <https://orcid.org/0000-0002-1800-8460>,  
Hodges, K. I. ORCID: <https://orcid.org/0000-0003-0894-229X>,  
Seddon, J., Vanniere, B. ORCID: <https://orcid.org/0000-0001-8600-400X>,  
Haarsma, R. J., Schiemann, R. ORCID: <https://orcid.org/0000-0003-3095-9856>,  
Kapetanakis, D., Tourigny, E., Lohmann, K., Roberts, C. D. and Terray, L. (2022) Extratropical transition of tropical cyclones in a multiresolution ensemble of atmosphere-only and fully coupled global climate models. *Journal of Climate*, 35 (16). pp. 5283-5306. ISSN 1520-0442 doi: <https://doi.org/10.1175/JCLI-D-21-0801.1> Available at <https://centaur.reading.ac.uk/105122/>

It is advisable to refer to the publisher's version if you intend to cite from the work. See [Guidance on citing](#).

Published version at: <https://journals.ametsoc.org/view/journals/clim/aop/JCLI-D-21-0801.1/JCLI-D-21-0801.1.xml>  
To link to this article DOI: <http://dx.doi.org/10.1175/JCLI-D-21-0801.1>

Publisher: American Meteorological Society

All outputs in CentAUR are protected by Intellectual Property Rights law, including copyright law. Copyright and IPR is retained by the creators or other copyright holders. Terms and conditions for use of this material are defined in the [End User Agreement](#).

[www.reading.ac.uk/centaur](http://www.reading.ac.uk/centaur)

## **CentAUR**

Central Archive at the University of Reading

Reading's research outputs online

# **Extratropical transition of tropical cyclones in a multiresolution ensemble of atmosphere-only and fully coupled global climate models**

Alexander J. Baker<sup>1,\*</sup>, Malcolm J. Roberts<sup>2</sup>, Pier Luigi Vidale<sup>1</sup>, Kevin I. Hodges<sup>1</sup>, Jon Seddon<sup>2</sup>, Benoît Vannière<sup>1</sup>, Rein J. Haarsma<sup>3</sup>, Reinhard Schiemann<sup>1</sup>, Dimitris Kapetanakis<sup>3</sup>, Etienne Tourigny<sup>4</sup>, Katja Lohmann<sup>5</sup>, Christopher D. Roberts<sup>6</sup>, and Laurent Terray<sup>7</sup>

<sup>1</sup> National Centre for Atmospheric Science and Department of Meteorology, University of Reading, Reading, Berkshire, UK

<sup>2</sup> Met Office Hadley Centre, Exeter, Devon, UK

<sup>3</sup> Koninklijk Nederlands Meteorologisch Instituut, De Bilt, The Netherlands

<sup>4</sup> Earth Sciences Department, Barcelona Supercomputing Center, Barcelona, Spain

<sup>5</sup> Max Planck Institut für Meteorologie, Hamburg, Germany

<sup>6</sup> European Centre for Medium-Range Weather Forecasts (ECMWF), Reading, UK

<sup>7</sup> Climat, Environnement, Couplages et Incertitudes, Centre Européen de Recherche et de Formation Avancée en Calcul Scientifique (CERFACS), Toulouse, France

\* alexander.baker@reading.ac.uk

For submission to *Journal of Climate*

Corresponding author: Dr Alexander J. Baker

National Centre for Atmospheric Science

Department of Meteorology,

University of Reading

Earley Gate, Whiteknights Road, Reading, Berkshire RG6 6ES, UK

+44 (0) 118 377 762

1 **Abstract**

2 Tropical cyclones undergo extratropical transition (ET) in every ocean basin. Projected  
3 changes in ET frequency under climate change are uncertain and differ between basins, so  
4 multimodel studies are required to establish confidence. We used a feature-tracking algorithm  
5 to identify tropical cyclones and performed cyclone phase-space analysis to identify ET in an  
6 ensemble of atmosphere-only and fully coupled global model simulations, run at various  
7 resolutions under historical (1950–2014) and future (2015–2050) forcing. Historical  
8 simulations were evaluated against five reanalyses for 1979–2018. Considering ET globally,  
9 ensemble-mean biases in track and genesis densities are reduced in the North Atlantic and  
10 Western North Pacific when horizontal resolution is increased from ~100 to ~25km. At high  
11 resolution, multireanalysis-mean climatological ET frequencies across most ocean basins as  
12 well as basins’ seasonal cycles are reproduced better than in low-resolution models. Skill in  
13 simulating historical ET interannual variability in the North Atlantic and Western North  
14 Pacific is ~0.3, which is lower than for all tropical cyclones. Models project an increase in ET  
15 frequency in the North Atlantic and a decrease in the Western North Pacific. We explain  
16 these opposing responses by secular change in ET seasonality and an increase in lower-  
17 tropospheric, pre-ET warm-core strength, both of which are largely unique to the North  
18 Atlantic. Multimodel consensus about climate-change responses is clearer for frequency  
19 metrics than for intensity metrics. These results help clarify the role of model resolution in  
20 simulating ET and help quantify uncertainty surrounding ET in a warming climate.

21

## 22 **1. Introduction**

23 The impacts of tropical cyclones are not confined to the tropics. Their post-tropical evolution  
24 makes these storms an important natural hazard across the midlatitudes (Baker et al., 2021;  
25 Bieli et al., 2019; Evans et al., 2017; Jones et al., 2003; Keller et al., 2019). The poleward  
26 propagation of tropical cyclones and the occurrence of extratropical transition (ET) exposes  
27 populous regions where risks to life and infrastructure are high—Northeast United States,  
28 maritime and eastern Canada, Western Europe, and East Asia—to hurricane-force wind  
29 speeds and extreme precipitation (Evans et al., 2017). In the North Atlantic, tropical-origin  
30 systems reached Northeast North America and Europe almost every year since 1979 (Baker  
31 et al., 2021), including recent intense landfalls. For instance, Hurricane Sandy (22<sup>nd</sup>–29<sup>th</sup>  
32 October, 2012)—the fourth costliest (by inflation-adjusted losses) North Atlantic hurricane  
33 yet recorded (Weinkle et al., 2018)—caused devastation across the Northeast United States  
34 and eastern Canada (Blake et al., 2013). Ex-hurricane Ophelia (9<sup>th</sup>–15<sup>th</sup> October, 2017) led to  
35 loss of life and severe wind damage across Ireland, the United Kingdom, and Scandinavia  
36 (Rantanen et al., 2020; Stewart, 2018). At midlatitude landfall, both systems were post-  
37 tropical, having begun ET, but possessed hurricane-like intensities, the human and economic  
38 impacts of which were felt across substantial areas. In the Western North Pacific, Typhoon  
39 Nabi (29<sup>th</sup> August–12<sup>th</sup> September, 2005) impacted two thirds of Japan’s prefectures as both  
40 a tropical and transitioning cyclone before undergoing cyclolysis over Alaska (Harr et al.,  
41 2008). These events, along with the current lack of consensus regarding ET in a changing  
42 climate, heighten the urgency with which global studies of historical and near-future post-  
43 tropical cyclone activity are needed.

44

45 Tropical cyclones undergo ET in every ocean basin (Hart and Evans, 2001; Studholme et al.,  
46 2015; Wood and Ritchie, 2014; Zarzycki et al., 2017), but pronounced interannual variability  
47 (Baker et al., 2021) and basin-to-basin differences (Bieli et al., 2019) exist. Transitioning  
48 cyclones are also known to influence the large-scale circulation, such as Hurricane Debbie in  
49 1982 (Laurila et al., 2019), and excite or amplify downstream Rossby waves (Evans et al.,  
50 2017; Jones et al., 2003; Keller et al., 2019; Michaelis and Lackmann, 2019). These cyclone-  
51 wave interactions influence downstream weather (Grams and Blumer, 2015; Keller et al.,  
52 2019). Of those cyclones which undergo ET, an appreciable proportion reintensify under  
53 favourable environmental conditions, where appropriate phasing between the transitioning  
54 cyclone and the upper-tropospheric flow pattern enhances baroclinic instability (Keller et al.,

55 2019). During and after ET, baroclinicity (Evans et al., 2017) and diabatic heating (Rantanen  
56 et al., 2020) may reintensify the post-tropical cyclone.

57

58 Over the period of 1979–2018, statistically significant positive trends in the frequency of  
59 North Atlantic ET events exist in several, but not all, reanalysis datasets (Baker et al., 2021).  
60 Existing climate model projections underline the plausibility of increased tropical and post-  
61 tropical cyclone activity in the midlatitudes in response to anthropogenic warming. There is  
62 evidence that more frequent ET events may occur in the future in the North Atlantic (Baatsen  
63 et al., 2015; Haarsma et al., 2013; Liu et al., 2017; Michaelis and Lackmann, 2019) and  
64 Western North Pacific (Bieli et al., 2020) ocean basins, but no consensus yet exists across  
65 studies, modelling campaigns, and methodologies. Moreover, best-track data limitations,  
66 which are well documented (Chang and Guo, 2007; Delgado et al., 2018; Hagen et al., 2012;  
67 Vecchi and Knutson, 2008), engender substantial uncertainty in observed trends (Lanzante,  
68 2019; Moon et al., 2019). Additionally, natural, multidecadal variability in tropical-cyclone  
69 frequency is yet to be accounted for (Knutson et al., 2020). Although global climate models  
70 project reduced frequencies of tropical cyclones, more intense tropical cyclones are expected  
71 in response to twenty-first-century warming (Knutson et al., 2020), potentially allowing a  
72 higher proportion of cyclones to survive cooler midlatitude sea-surface temperatures  
73 experienced prior to and during ET (Michaelis and Lackmann, 2019). Other factors,  
74 particularly changes in shear, will also be important, with current evidence suggesting that  
75 these will undergo ET-favourable future changes (Jung and Lackmann, 2021; Liu et al.,  
76 2017; Michaelis and Lackmann, 2021). Increased future ET event frequency is also  
77 consistent with the projected expansion of tropical-cyclone genesis regions (Studholme et al.,  
78 2022), potentially reducing the mean displacement cyclones must undergo prior to  
79 midlatitude ET. Together, these changes imply an increase in post-tropical cyclone impacts  
80 across populated midlatitude regions, and idealised experiments suggest an increase in ET-  
81 related, high-impact weather across Europe (Jung and Lackmann, 2021), where our  
82 understanding of historical risks is developing (Baker et al., 2021). Studies of historical and  
83 future model simulations are therefore needed to assess both contemporary risk and future  
84 changes more comprehensively.

85

86 One aspect of climate model evaluation important for both tropical and extratropical cyclones  
87 is understanding the role of horizontal resolution in simulated climates, prompted by recent  
88 developments in high-performance computing and data-management facilities. With

89 increases in model resolution to approximately 25 km, improved fidelity is anticipated for  
90 many synoptic phenomena, particularly tropical and midlatitude cyclones, which ultimately  
91 feed back onto the large scale. Recent studies have now firmly established that increasing  
92 model resolution improves simulated tropical-cyclone frequency statistics across most ocean  
93 basins (Manganello et al., 2019; Roberts et al., 2020a), leads to a more realistic global spatial  
94 distribution (Roberts et al., 2020a; Roberts et al., 2015; Strachan et al., 2013), and results in  
95 more realistic simulated warm-core vertical structures (Vannière et al., 2020). Moreover,  
96 model resolution is a key constraint on the intensity which simulated cyclones may reach  
97 (Davis, 2018). It is anticipated that atmospheric resolutions of  $\sim 50$  km or finer ( $\sim 0.25^\circ$   
98 ocean-model resolution) will yield improvement in the simulation of post-tropical cyclones  
99 and ET (Haarsma, 2021). However, no systematic multimodel studies of ET have been  
100 undertaken, and the impact of increasing model resolution (atmosphere and ocean) on  
101 simulated ET is also yet to be quantified. We address these issues in this paper using model  
102 simulations from the 6<sup>th</sup> phase of the Coupled Model Intercomparison Project (CMIP6),  
103 which follow an experimental protocol designed to isolate the impacts of changes in model  
104 resolution.

105

106 In this study of the representation of tropical cyclones undergoing ET across a multimodel  
107 ensemble, we focus on climatological statistics, interannual variability, and cyclone structure  
108 and intensity. These analyses are centred around two questions. What is the impact of  
109 increasing model atmospheric resolution on simulated ET? What changes in ET metrics  
110 under climate change are consistent across models? This paper continues in section 2 with a  
111 description of the model and reanalysis data as well as the cyclone-tracking and analysis  
112 methodologies. Our results are presented in section 3 and our conclusions are summarised,  
113 with further discussion, in section 4.

114

115

## 116 **2. Data and methodology**

### 117 *2.1 Reanalysis data*

118 Tropical cyclone best-track datasets are not well suited to analysis of cyclones undergoing ET  
119 because there are known heterogeneities within individual datasets (Barcikowska et al., 2012;  
120 Chu et al., 2002; Kossin et al., 2007; Vecchi and Knutson, 2008, 2011), especially for storms'  
121 post-tropical stages, under-counting biases (Chang and Guo, 2007; Delgado et al., 2018;  
122 Hagen et al., 2012), and differences between operational centres' data-collection

123 methodologies (Hodges et al., 2017; Schreck III et al., 2014). We therefore evaluated model  
124 simulations against five global reanalyses (Table 1): the European Centre for Medium-Range  
125 Weather Forecasts' Interim Reanalysis (ERA-Interim; Dee et al., 2011) and Fifth Reanalysis (ERA5;  
126 Hersbach et al., 2020); the Japanese 55-year Reanalysis (JRA55; Kobayashi et al., 2015); the  
127 National Aeronautics and Space Administration's Modern-Era Retrospective Analysis for  
128 Research and Applications version 2 (MERRA2; Molod et al., 2015); and the combined  
129 National Centers for Environmental Prediction Climate Forecast System Reanalysis and  
130 Climate Forecast System version 2 dataset (NCEP; Saha et al., 2014)—the sole fully coupled  
131 (atmosphere, ocean, land surface, and sea ice) reanalysis used herein. Between reanalyses,  
132 differing forecast model formulations and resolutions (horizontal and vertical), as well as  
133 data-assimilation schemes lead to differences in the representation of tropical-cyclone  
134 vertical structure, which was examined by Hodges et al. (2017). Baker et al. (2021) found  
135 that interannual variability in the number ET events is well correlated between reanalyses,  
136 but the percentage of tropical cyclones undergoing ET agrees less well between reanalyses on  
137 the interannual timescale. It is therefore necessary to consider multiple reanalyses as an  
138 observation-based reference, against which models may be evaluated.  
139



| Reanalysis    | Analysis period | Analysis grid | Model resolution<br>(grid spacing) | Data assimilation      | Sample sizes<br>( $n_{NH}$ , $n_{SH}$ ) |
|---------------|-----------------|---------------|------------------------------------|------------------------|---|
| <b>ERA5</b>   | 1979–2017       | 512x256       | TL255L60<br>(80 km)                | 4D-Var.                | 35.4, 37.0                              |
| <b>ERA5</b>   | 1979–2018       | 1140x721      | T639L137<br>(33km)                 | 4D-Var.                | 35.4, 37.0                              |
| <b>JRA55</b>  | 1959–2017       | 288x145       | TL319L60<br>(55 km)                | 4D-Var.                | 35.4, 37.0                              |
| <b>MERRA2</b> | 1980–2016       | 576x361       | Cubed sphere<br>(50 km)            | 3D-Var. + GSI +<br>IAU | 35.4, 37.0                              |
| <b>NCEP</b>   | 1979–2016       | 720x361       | T382L64<br>(38 km)                 | 3D-Var. + GSI          | 35.4, 37.0                              |

142 **Table 1.** Reanalyses. Atmospheric mesh spacing at 50 °N in units of km is given in brackets.  
143 3(4)D-Var.: 3(4)D variational data assimilation; GSI: Grid-point Statistical Interpolation;  
144 IAU: Incremental Analysis Update. The representation of tropical and post-tropical cyclones  
145 in these reanalyses were evaluated by Hodges et al. (2017) and (Baker et al., 2021),  
146 respectively. Annual-mean global sample sizes (cyclones year<sup>-1</sup>) for all tropical cyclones  
147 undergoing ET for each reanalysis are given as  $n_{NH}$ ,  $n_{SH}$ .  
148

## 149 2.2 The multiresolution PRIMAVERA model ensemble

150 We evaluated CMIP6 High-Resolution Model Intercomparison Project (HighResMIP;  
151 Haarsma et al., 2016) historical and future atmosphere-only (Tier 1 and Tier 3, respectively),  
152 including interaction with the land surface, and fully coupled (Tier 2) simulations from five  
153 global climate models (Table 2): CNRM-CM6.1 (Voldoire et al., 2019), EC-Earth3P  
154 (Haarsma et al., 2020), ECMWF-IFS (cycle 43r1; Roberts et al., 2018), HadGEM3-GC3.1  
155 (Roberts et al., 2019; Williams et al., 2018), and MPI-ESM1.2 (Gutjahr et al., 2019). Each  
156 model participated in the European Commission Horizon2020-funded project PRIMAVERA  
157 (PProcess-based climate sIMulation: AdVances in high-resolution modelling and European  
158 climate Risk Assessments; primavera-h2020.eu). Historical (1950–2014) and future (2015–  
159 2050) atmosphere-only experiments are termed *highresSST-present* and *highresSST-future*,  
160 respectively, and fully coupled experiments are termed *hist-1950* and *highres-future*,  
161 respectively. Historical *highresSST-present* simulations were forced by HadISST2 daily sea-  
162 surface temperature (SST) at a resolution of  $0.25^\circ$  interpolated to each model's grid (no  
163 ocean mixed-layer model). Out to 2050, *highresSST-future* simulations were forced  
164 according to Representative Concentration Pathway 8.5 (RCP8.5). (Use of RCP8.5 allowed  
165 modelling centres to begin their model simulations before Shared Socioeconomic Pathways  
166 scenarios became available.) In HighResMIP, future simulations were performed with all  
167 models except ECMWF-IFS. The rate of projected sea-surface temperature (SST) warming  
168 was derived from an ensemble mean of CMIP5, with interannual variability derived from the  
169 historical period 1950–2014 (Haarsma et al., 2016).

170

171 Under the HighResMIP experimental protocol, minimal changes in model-tuning parameters  
172 were made between low- and high-resolution integrations to ensure that resolution-sensitivity  
173 studies were not confounded by substantial differences in model configurations between  
174 resolutions (Haarsma et al., 2016). Between low- and high-resolution configurations, no  
175 model-physics changes were made to the atmospheric components of CNRM-CM6.1 and  
176 EC-Earth3P, but minor adjustments were made to a single parameter in ECMWF-IFS (related  
177 to net surface energy balance), HadGEM3-GC3.1 (related to quasi-biennial oscillation  
178 period), and MPI-ESM1.2 (related to numerical stability). For the ocean model in coupled  
179 configurations, one key difference is the effects of mesoscale eddies are parameterised at low  
180 resolution ( $\sim 1^\circ$ ) but partially resolved at high resolution ( $\sim 0.25^\circ$ ) (e.g., Roberts et al., 2018;  
181 Roberts et al., 2019). For all models, shorter dynamical timesteps were used in the high-  
182 resolution integrations to ensure numerical stability. The effective resolutions of the high-

183 resolution model configurations, measured by kinetic energy spectra, resolve synoptic-scale  
184 dynamics (Klaver et al., 2020). Since this study concerns cyclone translation from the tropics  
185 to the extratropics, resolutions are given as a model's regular mesh spacing at a latitude of 50  
186 ° (Table 2). For convenience, we refer to resolutions nominally (i.e., 'low' or 'high') as well  
187 as quantitatively, where necessary. A single ensemble member was analysed at each  
188 resolution for both the atmosphere-only and fully coupled experiments.  
189

| <b>Atmospheric model</b> | <b>Ocean model</b> | <b>Atmospheric dynamical core</b>             | <b>Resolution nomenclature</b> | <b>Atmospheric resolution</b> | <b>Atmospheric mesh spacing</b> |
|--------------------------|--------------------|---|--------------------------------|-------------------------------|---------------------------------|
| ARPEGE6.3                | NEMO               | Spectral (linear, reduced Gaussian)           | LR; HR                         | TL127; TL359                  | 142; 50 km                      |
| IFS cyc36r4              | NEMO               | Spectral (linear, reduced Gaussian)           | LR; HR                         | TL255; TL511                  | 71; 36 km                       |
| IFS cyc43r1              | NEMO3.4            | Spectral (cubic octahedral; reduced Gaussian) | LR; HR                         | Tco199; Tco399                | 50; 25 km                       |
| MetUM                    | NEMO               | Grid point (SISL)                             | LM (LL); MM; HM (HH)           | N96; N216; N512               | 135; 60; 25 km                  |
| ECHAM6.3                 | MPIOM1.63          | Spectral (triangular; Gaussian)               | HR; XR                         | T127; T255                    | 67; 34 km                       |

| <b>Model name</b> | <b>CNRM-CM6.1</b> | <b>EC-Earth3P</b> | <b>ECMWF-IFS</b> | <b>HadGEM3-GC3.1</b> | <b>MPI-ESM1.2</b> |
|-------------------|-------------------|-------------------|------------------|----------------------|-------------------|
|-------------------|-------------------|-------------------|------------------|----------------------|-------------------|

190

191 **Table 2.** The PRIMAVERA (HighResMIP) model ensemble. NEMO: Nucleus for European  
 192 Modelling of the Ocean. MPIOM: Max Plank Institute Ocean Model. SISL: semi-implicit,  
 193 semi-Lagrangian. For fully coupled simulations, the LL and HH configurations of  
 194 HadGEM3-GC3.1 were also included; LL denoting low-resolution atmosphere and low-  
 195 resolution (1 °) ocean and HH denoting high-resolution atmosphere and high-resolution (1/12  
 196 °) ocean. Atmosphere mesh spacing is given for 50 °N. Sample sizes for all tropical cyclones  
 197 undergoing ET across this ensemble are given in Table 3. DOIs for each simulation are listed  
 198 at [primavera-h2020.eu/modelling/](http://primavera-h2020.eu/modelling/).

199

### 200 2.3 Lagrangian tropical-cyclone tracking

201 To identify and track the evolution of tropical cyclones, we used the objective feature-  
202 tracking algorithm—TRACK—of Hodges (1995), a well-established tool for identifying  
203 cyclones in reanalyses (Hodges et al., 2017) and model simulations (Roberts et al., 2020a).  
204 The TRACK algorithm was applied to six-hourly relative vorticity, computed from the zonal  
205 and meridional wind fields, which was vertically averaged over the 850-, 700- and 600-hPa  
206 levels and spectrally filtered. (Upper-level vorticity is used in subsequent identification.)  
207 Filtering to the T5–T63 spectral band removes both large, planetary scales (total  
208 wavenumbers 0–5) and small-scale noise (total wavenumbers >63). Vorticity maxima  
209 exceeding  $0.5 \times 10^{-5} \text{ s}^{-1}$  (in the Northern Hemisphere; scaled by  $-1$  in the Southern  
210 Hemisphere) were identified, initialised into tracks using a nearest-neighbour approach, and  
211 subsequently refined by minimising a cost function for track smoothness, subject to adaptive  
212 constraints on track displacement and smoothness (Hodges, 1995, 1999). The use of  
213 vertically averaged vorticity improves temporal coherence in instances where vorticity  
214 maxima shift between levels (Hodges et al., 2017).

215

216 Cyclone-centred sampling of meteorological fields along cyclone tracks was performed to  
217 detect warm-core structures and measure cyclone intensities, following Hodges et al. (2017).  
218 For warm-core identification, the T63-truncated vorticity data on seven levels covering 850–  
219 250 hPa were added to tracks by recursively searching for a vorticity maximum at each level  
220 using the previous level’s maximum as the starting point for a steepest-ascent maximization  
221 applied to the B-spline-interpolated field. A search radius of  $5^\circ$  was used, centred on each  
222 level’s maximum. For the Southern Hemisphere, fields were scaled by  $-1$ . To quantify  
223 cyclone intensity, mean sea-level pressure minima within a radius of  $5^\circ$  and 925-hPa and 10-  
224 metre wind speed maxima within a radius of  $6^\circ$  of the storm centre were sampled from  
225 reanalysis or model-output fields at their native, non-truncated resolutions. (All radii are  
226 geodesic.)

227

228 Following Hodges et al. (2017), objective identification of tropical cyclones adhered to the  
229 following criteria:

- 230     ▪ cyclogenesis equatorward of  $30^\circ\text{N}$
- 231     ▪ total cyclone lifetime must exceed two days
- 232     ▪ T63 relative vorticity at 850 hPa must exceed  $6 \times 10^{-5} \text{ s}^{-1}$

- 233       ▪ T63 relative vorticity centre must exist at each level between 850 and 250 hPa to  
234       indicate a coherent vertical structure
- 235       ▪ T63 relative vorticity decrease with increasing height between 850 and 250 hPa by at  
236       least  $6 \times 10^{-5} \text{ s}^{-1}$  to indicate the presence of a warm core

237 The three T63 relative vorticity criteria must also be jointly attained for at least four  
238 consecutive time steps (i.e., one day) over ocean only. Together, these criteria minimise  
239 inclusion of spurious short-lived or relatively weak vorticity features. The same criteria were  
240 used for each reanalysis and model simulation and across all ocean basins.

241

242 Crucial to our analyses, vorticity-based tracking and post-tracking identification of tropical  
243 cyclones yields longer cyclone lifecycles (compared with central-pressure-based algorithms  
244 and methodologies where identification is performed during tracking), which allows for  
245 objective analysis of post-tropical storm evolution (Hodges et al., 2017). A comparison of  
246 TRACK results with results from a different tracking algorithm, which does not capture the  
247 full lifecycle, demonstrates this advantage of vorticity-based tracking (section S1.1; Fig. S1).  
248 In addition, filtering gridded data to a common spectral truncation, rather than tuning the  
249 cyclone-tracking algorithm to a given dataset, allows both inter-model and inter-resolution  
250 comparisons that are not complicated by methodological differences (Hodges et al., 2017).  
251 Applying TRACK to a reanalysis globally, as described here, identifies  $\sim 30,000$  tropical  
252 vortices per year. Of these,  $\sim 8,000$  per year have a lifetime that exceeds two days and are  
253 retained; of these,  $\sim 120$  per year exhibit the warm-core structure of a tropical cyclone  
254 (Vannière et al., 2020). Our study is based on recently published tropical cyclone track  
255 datasets, derived using a consistent methodology (Roberts et al., 2020a; Roberts et al.,  
256 2020b). Sample sizes for all tropical cyclones undergoing ET are given in Table 3. Finally,  
257 spatial track statistics—track and genesis densities—were computed using spherical kernel  
258 estimators, following Hodges (1996).

259



| Model name       | Atmosphere-only           |                          | Fully coupled    |                       |
|------------------|---------------------------|--------------------------|------------------|-----------------------|
|                  | <i>highresSST-present</i> | <i>highresSST-future</i> | <i>hist-1950</i> | <i>highres-future</i> |
| CNRM-CM6.1       | 42.3, 52.0                | 41.0, 47.5               | 43.4, 45.8       | 40.1, 39.4            |
| CNRM-CM6.1-HR    | 47.9, 55.9                | 46.7, 51.5               | 50.0, 49.6       | 46.8, 42.3            |
| EC-Earth3P       | 19.2, 29.3                | 20.1, 28.9               | 19.9, 27.6       | 19.1, 24.0            |
| EC-Earth3P-HR    | 30.1, 32.1                | 29.1, 29.4               | 26.6, 28.8       | 26.8, 27.8            |
| ECMWF-IFS-LR     | 34.7, 41.6                | n/a                      | 29.6, 41.5       | n/a                   |
| ECMWF-IFS-HR     | 39.8, 44.6                | n/a                      | 34.5, 41.7       | n/a                   |
| HadGEM3-GC3.1-LL | n/a                       | n/a                      | 28.4, 38.7       | 28.6, 36.3            |
| HadGEM3-GC3.1-LM | 36.3, 50.0                | 36.5, 50.7               | n/a              | n/a                   |
| HadGEM3-GC3.1-MM | 60.1, 68.8                | 60.9, 65.0               | 55.0, 56.0       | 53.2, 53.4            |
| HadGEM3-GC3.1-HM | 63.8, 69.0                | 63.1, 64.6               | 58.1, 56.4       | 58.9, 54.3            |
| HadGEM3-GC3.1-HH | n/a                       | n/a                      | 63.4, 56.2       | 60.1, 52.9            |
| MPI-ESM1.2-HR    | 10.5, 16.0                | 9.4, 14.5                | 11.4, 16.9       | 10.4, 15.5            |
| MPI-ESM1.2-XR    | 10.1, 17.0                | 9.6, 15.0                | 11.1, 17.4       | 10.1, 14.9            |

260

261 **Table 3.** Annual-mean global sample sizes (cyclones year<sup>-1</sup>) for all tropical cyclones  
262 undergoing ET in each model simulation, given as  $n_{NH}$ ,  $n_{SH}$ .

263

264 2.4 Cyclone phase-space analysis

265 The temporal evolution of cyclone structure, including identifying ET, is quantifiable by  
 266 analysis of a cyclone’s thermal wind fields (Hart, 2003; Hart and Evans, 2001). So-called  
 267 cyclone phase-space analysis involves three parameters: the thermal axisymmetry of the  
 268 cyclone ( $B$ ; Eq. 1) and the lower- ( $T_L$ ; Eq. 2) and upper-tropospheric ( $T_U$ ; Eq. 3) cyclone-  
 269 relative thermal winds. In this study, these parameters were computed using 6-hourly data for  
 270 all reanalyses and climate models.  $B$  is defined as:

$$271 \quad B = h \left( \overline{Z_{600} - Z_{925}} \Big|_R - \overline{Z_{600} - Z_{925}} \Big|_L \right) \quad (1)$$

272 where  $h = 1$  for the Northern Hemisphere and  $-1$  for the Southern Hemisphere,  $Z_p$  is  
 273 geopotential height (m) at level  $p$  (isobaric; hPa), and  $R$  and  $L$  denote the right- and left-hand  
 274 semicircles, respectively, relative to the cyclone’s displacement direction. In this study, we  
 275 followed the majority of previous research (Bieli et al., 2019; Bieli et al., 2020; Dekker et al.,  
 276 2018; Hart, 2003; Liu et al., 2017; Studholme et al., 2015) and defined thermal axisymmetry  
 277 (i.e., non-frontal) as  $B < 10$  and asymmetry (i.e., frontal) as  $B \geq 10$  m. To compute  $T_L$  and  $T_U$   
 278 between isobaric surfaces, Hart (2003) used the slope of the linear regression between  $\Delta Z$  and  
 279  $\ln p$  as the derivative of  $\Delta Z$  relative to  $\ln p$  to determine the mean  $\Delta Z$  over a given pressure  
 280 range. However, to ensure consistency between phase-space parameters computed from  
 281 reanalyses and model output, and to account for the different pressure levels on which  
 282 reanalysis and model data are available, it was necessary to adopt a three-level procedure,  
 283 following recent studies (Bieli et al., 2019; Bieli et al., 2020; Liu et al., 2017; Studholme et  
 284 al., 2015). Here,  $T_L$  (925–600 hPa) and  $T_U$  (600–250 hPa) are defined as vertical derivatives  
 285 of the horizontal geopotential height gradient:

$$286 \quad T_L \equiv -|V_T^L| = \frac{\partial(\Delta Z)}{\partial \ln p} \Big|_{925 \text{ hPa}}^{600 \text{ hPa}} \quad (2)$$

$$287 \quad T_U \equiv -|V_T^U| = \frac{\partial(\Delta Z)}{\partial \ln p} \Big|_{600 \text{ hPa}}^{250 \text{ hPa}} \quad (3)$$

288 where  $p$  is pressure and  $\Delta Z = Z_{max} - Z_{min}$ , where  $Z_{max}$  and  $Z_{min}$  are the maximum and minimum  
 289 geopotential height, respectively, at a given level within a  $5^\circ$  radius of the cyclone centre.  
 290 Positive  $T_L$  or  $T_U$  indicates the presence of a warm core in the upper or lower troposphere,  
 291 respectively; negative values indicate a cold core. A deep warm- or cold-core structure is  
 292 identified where  $T_L$  and  $T_U$  have the same sign. We performed phase-space analysis for all  
 293 reanalyses (section 2.1) and all PRIMAVERA models (section 2.2). In our analysis, cyclone  
 294 centres in reanalyses and model output are those identified objectively by TRACK, which

295 ensures dynamical consistency between cyclone positions and the geopotential height field.  
296 This differs from Bieli et al. (2020), who centred reanalysis geopotential data on best-track  
297 storm locations. The approach taken in our study avoids any potential inconsistencies  
298 between reanalysis and best-track storm centres, which would need to be accounted for,  
299 particularly at weaker intensities (Hodges et al., 2017).

300

301 Among existing studies, various phase-space thresholds have been employed to identify ET  
302 (e.g., Bieli et al., 2019; Hart and Evans, 2001; Kofron et al., 2010; Liu et al., 2017; Zarzycki  
303 et al., 2017). We defined ET onset as either cold-core development (i.e.,  $T_L < 0$ ) or  
304 development of thermal asymmetry (i.e.,  $B \geq 10$ ), thereby allowing for either ET pathway. ET  
305 completion is defined as the first occurrence of both  $B \geq 10$  m and  $T_L < 0$ . These thresholds  
306 are suitable for high-resolution gridded data (Michaelis and Lackmann, 2019) and are  
307 supported by cluster analysis of observed ET events (Arnott et al., 2004). However, much of  
308 the ET-identification literature has focussed on the North Atlantic, yet ET phase-space  
309 pathways may differ between ocean basins (Bieli et al., 2019). To account for these  
310 difficulties in our global study, ET was identified only where the completion criterion is  
311 satisfied for at least four consecutive timesteps (i.e., one day). The use of this additional one-  
312 day criterion identifies meaningful temporal changes in  $B$  and  $T_L$  and avoids counting any  
313 spurious, high-frequency temporal variability in phase-space parameters as multiple core-  
314 structure changes, following (Baker et al., 2021). An analysis of the sensitivity of ET location  
315 to methodological choices is presented in section S1.2, showing a large spread in ET location  
316 (Fig. S2). In this study, ET-completion latitude was identified after a warm-core structure  
317 persisted for at least 2 days based on phase-space parameters (i.e.,  $T_L > 0$  and  $T_U > 0$ ),  
318 corresponding to ‘ $w$ ’ in Fig. S2. As such, sample sizes (Table 1 and Table 3) remain  
319 unchanged. This method avoids false positives in ET identification arising from tropical  
320 depressions and other weak, precursor systems (Bieli et al., 2020), and is therefore more  
321 appropriate to analysis of ET location (see section S1.2 for details).

322

323

### 324 *2.5. Identifying post-ET reintensification*

325 Instances of post-ET reintensification were defined as a post-ET increase in  $p_{min}$  of at least  $-4$   
326 hPa, a threshold that is based on published case studies (e.g., Zhu et al., 2018), but the  
327 number of identified reintensification events is necessarily sensitive to this threshold. For  
328 consistency, we applied a single threshold across all reanalyses and models; a higher

329 threshold will likely be appropriate for any future analysis of higher-resolution (i.e.,  
330 convection-permitting) models. We used  $p_{min}$  to avoid any complications arising from inter-  
331 model differences in how near-surface wind speeds are computed (e.g., related to surface  
332 roughness).

333

334

### 335 *2.6 Eady growth rate*

336 Eady growth rate maxima (Eq. 4) were computed as (Hoskins and Valdes, 1990):

$$337 \sigma_{max} = 0.31 \frac{f}{N} \frac{\partial(u,v)}{\partial Z} \quad (4)$$

338 where  $f$  is the Coriolis parameter,  $N$  is the static stability parameter,  $Z$  is geopotential height,  
339 and  $u$  and  $v$  are the zonal and meridional winds, respectively, which were used to compute  
340 the magnitude of the horizontal wind (i.e.,  $\sqrt{u^2 + v^2}$ ). The vertical derivatives,  $\partial(u,v)$  and  $\partial Z$ ,  
341 were computed between the 850- and 250-hPa levels using 6-hourly data.

342

343

## 344 **3. Results**

345 In each of the following sections, we present historical results and model evaluation followed  
346 by analysis of projected future changes out to 2050.

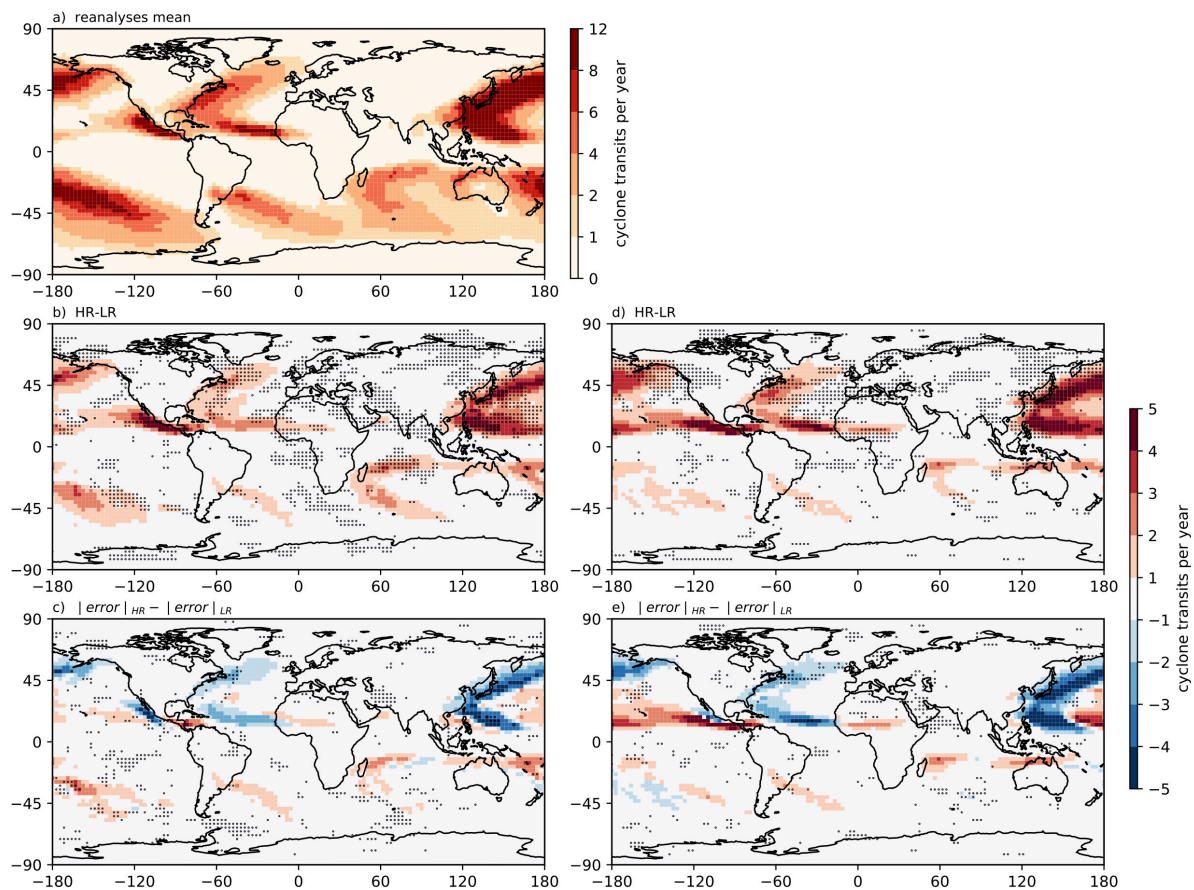
347

348

### 349 *3.1 Spatial cyclone statistics*

350 We first present spatial track density patterns for tropical cyclones undergoing ET in  
351 reanalyses and simulated across the PRIMAVERA ensemble. Reanalyses exhibit a high  
352 degree of consistency for track density and demonstrate that tropical cyclones undergo ET in  
353 all ocean basins. However, fewer ET events are identified over the Northern Indian Ocean  
354 (Fig. 1a), where relatively low-latitude landfall either disrupts liminal ET events or averts  
355 potential ET cases altogether, primarily via boundary-layer frictional effects (Bieli et al.,  
356 2019). Overall, basins' climatological ET activity is proportional to their tropical cyclone  
357 activity. The highest ET frequencies are identified in both the Western North Pacific and  
358 South Pacific basins, with climatological mean values of  $\sim 12$  cyclones year<sup>-1</sup>. The North  
359 Atlantic is the most active basin for ET outside the Pacific, and comparably low activity  
360 occurs across the South Atlantic and South Indian basins (Fig. 1a).

361



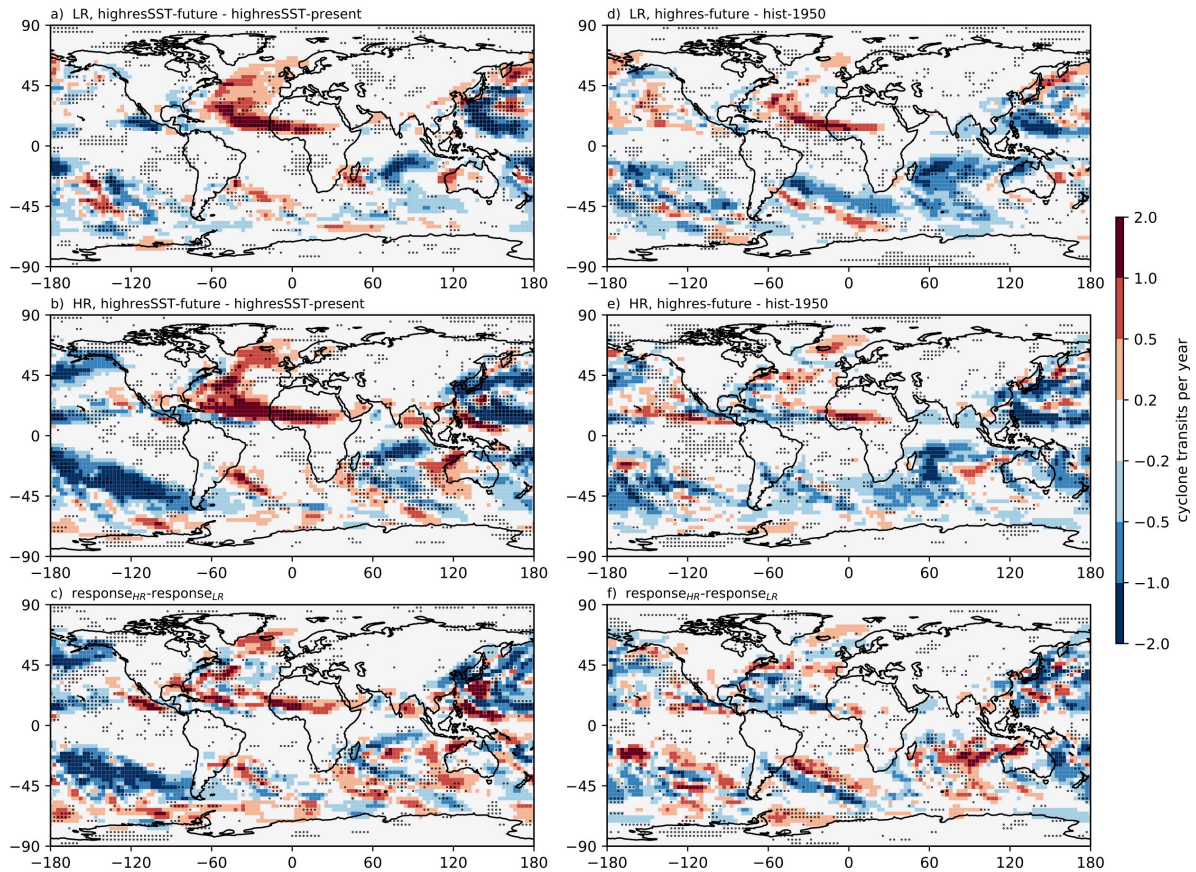
362

363 **Fig. 1.** Cyclone track density for all tropical cyclones undergoing ET. (a) Multireanalysis  
 364 mean, (b–c) *highresSST-present* and (d–e) *hist-1950*. Track density was computed from  
 365 complete tracks, including precursor stages, and is shown in units of cyclone transits per year  
 366 per unit area (within a  $5^\circ$  geodesic radius of storm centres). All available reanalysis years  
 367 (Table 1) are included in this analysis. (b, d) HR–LR denotes the ensemble-mean difference  
 368 between high and low resolution. (c, e)  $|\text{error}|_{\text{HR}} - |\text{error}|_{\text{LR}}$  denotes the ensemble-mean  
 369 difference of the absolute error (model versus multireanalysis mean) between high and low  
 370 resolution. The low-resolution (‘LR’) sub-ensemble includes CNRM-CM6.1-LR, EC-  
 371 Earth3P-LR, ECMWF-IFS-LR, HadGEM3-GC3.1-LM(-LL), and MPI-ESM1.2-HR. The  
 372 high-resolution (‘HR’) sub-ensemble includes CNRM-CM6.1-HR, EC-Earth3P-HR,  
 373 ECMWF-IFS-HR, HadGEM3-GC3.1-HM(-HH), and MPI-ESM1.2-XR. In b)–e), stippling  
 374 indicates where all five models agree on the sign of the difference.

375

376 The frequency of ET events simulated by PRIMAVERA models increases when resolution is  
377 increased from  $\sim 100$  km to  $\sim 25$  km in all basins, both in the *highresSST-present* (Fig. 1b) and  
378 *hist-1950* (Fig. 1d) experiments. Ensemble-mean climatologies are similar between both  
379 experiments (Fig. S3). The North Atlantic and Western North Pacific basins are regions of  
380 relatively widespread inter-model agreement on the sign of this resolution-sensitivity in track  
381 density, again regardless of whether SST is prescribed. When prescribed, inter-model  
382 agreement is also identified in the South Pacific and South Indian basins (Fig. 1b). This result  
383 is consistent with a recent equivalent analysis of all tropical cyclones in PRIMAVERA  
384 simulations (Roberts et al., 2020a), where increased frequencies were simulated at higher  
385 model resolution across all ocean basins, for which the leading explanation is that finer  
386 atmospheric resolution increases the conversion rate of precursor vortices (or ‘seeds’) to  
387 tropical cyclones (Roberts et al., 2020a; Vecchi et al., 2019; Vidale et al., 2021). Tropical-  
388 cyclone intensities simulated at model resolutions in the range 50–20 km are more  
389 comparable with observational estimates (Roberts et al., 2020a), due in part to enhanced  
390 surface latent heat flux (Vannière et al., 2020), implying that a more realistic proportion may  
391 withstand midlatitude environmental conditions hostile to tropical cyclones prior to and  
392 during the initial stages of ET. At low resolutions (typically  $\sim 100$  km), PRIMAVERA models  
393 simulate too few ET systems compared with reanalyses, particularly across the North Atlantic  
394 and Western North Pacific, in both the *highresSST-present* (Fig. S4a) and *hist-1950* (Fig.  
395 S4c) experiments. Increasing resolution to  $\sim 25$  km leads to increased track density globally,  
396 reducing negative biases in these basins but engendering positive biases in the Eastern North  
397 Pacific and South Pacific (Fig. S4c, d). In *hist-1950*, this bias reduction is consistent with a  
398 reduction in negative surface temperature biases at high resolution (e.g.,  $\sim 1$  °K reduction in  
399 the North Atlantic; Moreno-Chamarro et al., 2022). In section 3.2, we examine ET frequency  
400 and the percentage of tropical cyclones undergoing ET separately.

401



402

403

404

405

406

407

408

409

410

411

**Fig. 2.** Climate-change response of track density for all cyclones undergoing ET. (a–c) *highresSST-future* minus *highresSST-present* and (d–f) *highres-future* minus *hist-1950*. Track density was computed from complete tracks, including precursor stages, and is shown in units of cyclone transits per year per unit area (within a 5° geodesic radius of storm centres). The low-resolution (‘LR’) sub-ensemble includes CNRM-CM6.1-LR, EC-Earth3P-LR, HadGEM3-GC3.1-LM(-LL), and MPI-ESM1.2-HR. The high-resolution (‘HR’) sub-ensemble includes CNRM-CM6.1-HR, EC-Earth3P-HR, HadGEM3-GC3.1-HM(-HH), and MPI-ESM1.2-XR. Stippling indicates where all models agree on the sign of the difference.

412 Overall, PRIMAVERA simulations indicate that increasing resolution improves the  
413 representation of ET frequency, as measured by track density, particularly across the North  
414 Atlantic and Western North Pacific (Fig. 1c, e). For these basins, reductions in ensemble-  
415 mean absolute biases are found in both *highresSST-present* and *hist-1950*, and areas of bias  
416 reduction across multiple models occur primarily over western boundary currents—the Gulf  
417 Stream and Kuroshio, respectively. That these regions of resolution-dependence and reduced  
418 biases overlap indicates that capturing the sharpness of SST fronts and associated  
419 baroclinicity is important in simulating ET (Evans et al., 2017; Klein et al., 2002), and,  
420 consistent with this, we find enhanced meridional SST gradients in both of these boundary-  
421 current regions (Fig. S5). In the Southern Hemisphere, little difference in ensemble-mean  
422 biases is found between resolutions, with a caveat that observational or reanalysis-based  
423 climatologies for the Southern Ocean are themselves more uncertain (Hodges et al., 2017).  
424 The PRIMAVERA ensemble provides evidence that atmospheric resolutions typical of  
425 CMIP6 are too coarse to adequately capture basin-mean tropical-cyclone (Roberts et al.,  
426 2020a) and ET statistics (this study). Increasing resolution to ~25 km partly addresses this  
427 shortcoming.

428

429 The climate-change response of track density for tropical cyclones undergoing ET in high-  
430 resolution simulations is basin-dependent, with differences between atmosphere-only and  
431 fully coupled simulations also apparent. In *highresSST-future*, increased track density is  
432 simulated across the North and South Atlantic (but decreased over the eastern United States)  
433 and over the Maritime Continent; decreases are simulated over the Eastern and Western  
434 North Pacific and South Indian basins; and an unclear, mixed response characterises the  
435 North Indian Ocean (Fig. 2a–b). Inter-model agreement about the sign of these changes is  
436 largely confined to cyclogenesis regions (e.g., equatorial West Africa) and over the Gulf  
437 Stream and Kuroshio Current. In *highres-future* simulations, positive climate-change  
438 responses are confined to the central and Eastern North Pacific. The spatial response pattern  
439 over the North Atlantic—increased over central and eastern North Atlantic and decreased  
440 along the United States’ east coast—is similar between *highresSST-future* and *highres-future*,  
441 but the magnitude of the response is reduced in the fully coupled simulations (Fig. 2d–f).  
442 This spatial pattern is supported by recent projections, with increases particularly apparent in  
443 the eastern North Atlantic (Liu et al., 2017), consistent with the projected eastward and  
444 poleward expansion of cyclogenesis within this basin (Haarsma et al., 2013).

445



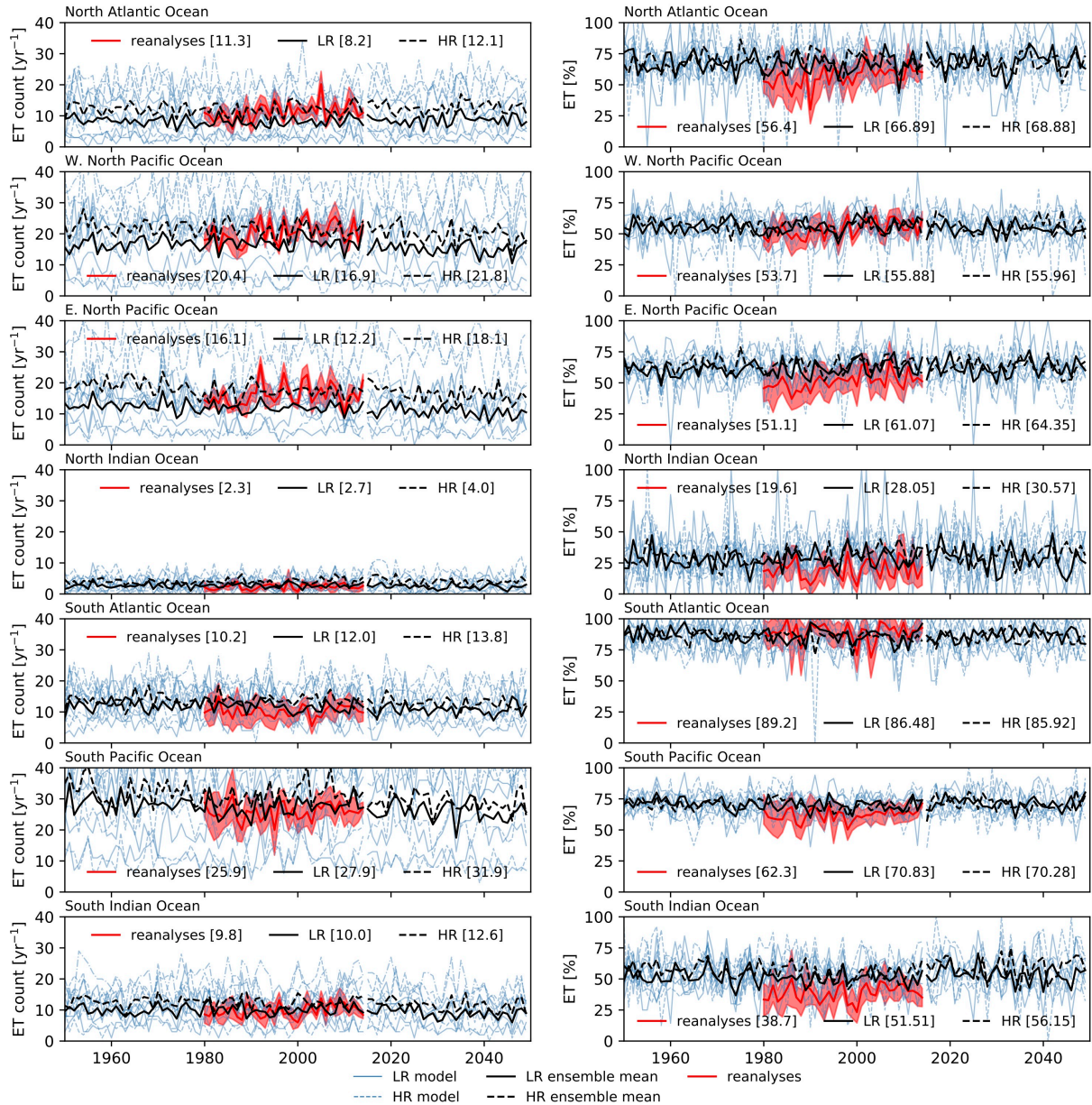
446 Increasing horizontal resolution has a localised effect on the climate-change response of track  
447 density for ET (Fig. 2c, f). In *highresSST-future*, resolution-sensitive responses to climate  
448 change, which are common across *all* models, are seen only over the central North Atlantic  
449 and parts of the Southern Ocean. In *highres-future*, spatially coherent and resolution-sensitive  
450 responses to climate change are seen over the South Atlantic and Eastern North Pacific  
451 basins, where simulated track density maxima are shifted equatorward at high resolution.  
452 However, the spatial patterns of resolution sensitivity over the North Atlantic and Western  
453 North Pacific broadly resemble the spatial climate-change response patterns, which indicates  
454 that these responses are enhanced at high resolution in most models. This is seen more clearly  
455 in the atmosphere-only experiment (Fig. 2c) than in the fully coupled experiment (Fig. 2f).

456  
457

### 458 *3.2 Interannual variability in ET*

459 Over the period 1979–2018, high-resolution *highresSST-present* simulations reproduce the  
460 multireanalysis-mean climatological ET counts for Northern Hemisphere basins (Fig. 3, left),  
461 except for the Northern Indian Ocean, a basin where few ET events occur. However, little  
462 improvement with increased resolution is seen for Southern Hemisphere basins (Fig. 3, left).  
463 Again, uncertainty is higher across the Southern Ocean, with greater inter-reanalysis spread  
464 seen for Southern Hemisphere basins. These results are also true of the *hist-1950* simulations  
465 (Fig. 4, left). The *highresSST-present* simulations appear to capture decadal variability in the  
466 role of SST in sustaining tropical cyclones to ET. In certain basins, periods are apparent  
467 where the *highresSST-present* ensemble mean and multireanalysis mean ET count match  
468 well: e.g., 1985–2000 for the North Atlantic and 1990–2005 for the Western North Pacific  
469 (Fig. 3, left). These periods coincide with observed positive phases in Atlantic Multidecadal  
470 Variability and Pacific Decadal Oscillation, respectively. For ET %, differences between  
471 low- and high-resolution ensemble means are small for most basins (Fig. 3, right). This  
472 suggests that the large-scale environmental conditions conducive to ET are not substantially  
473 different across the range of model resolutions considered here. This indicates that increased  
474 ET frequency at high resolution is driven primarily by increased tropical cyclone frequency,  
475 not by an increase in ET %. Similar mean values and variance in ensemble-mean ET count  
476 and ET % are simulated in both *highresSST-present* (Fig. 3) and *hist-1950* (Fig. 4)  
477 experiments.

478



479

480

481

482

483

484

485

486

487

488

**Fig. 3.** Interannual variability in (left) the number of ET events and (right) the percentage of tropical cyclones undergoing ET in each ocean basin in reanalyses and simulated in *highresSST-present* and *highresSST-future* experiments. Shown are (red) the multireanalysis mean, with 1 standard deviation of the reanalysis spread indicated by red shading, and (solid black) low- and (dashed black) high-resolution ensemble means. Each panel's legend gives climatological-mean values of (left) ET count or (right) ET % for the reanalyses and historical simulations. Also shown are (blue) timeseries for individual simulations to indicate the ensemble spread for each basin.

489 In *highresSST-present*, models' skill in reproducing the multireanalysis-mean interannual  
490 variability in ET count varies between basins (Table 4). Interannual variability in ensemble-  
491 mean and multireanalysis-mean ET counts are significantly, positively correlated for three  
492 basins at low resolution and four basins at high resolution. The North Atlantic and Western  
493 North Pacific basins are significantly correlated at both resolutions; the South Atlantic and  
494 South Pacific basins are significantly correlated only at high resolution; and the Eastern  
495 North Pacific is significant only at low resolution. Only for the North and South Indian basins  
496 is ensemble-mean variability uncorrelated with reanalyses at either resolution. (Correlation  
497 coefficients for *hist-1950* simulations are not shown because it is not expected that fully  
498 coupled models' internal year-to-year variability would mimic that of forced simulations or  
499 reanalyses.) For ET %, fewer significant correlations are found between ensemble-mean and  
500 multireanalysis-mean timeseries (Table 4). Positive correlations are seen in the Northern and  
501 Southern Indian basins and in the South Pacific basin at high resolution. However, low- and  
502 high-resolution ensemble-mean ET % timeseries covary in most basins in both *highresSST-*  
503 *present* (Fig. 3) and *hist-1950* (Fig. 4), more so than for ET count. To explain this, we  
504 hypothesise that the large-scale environment conducive to the baroclinic conversion of  
505 tropical cyclones is less sensitive to model resolution, while ET count depends on tropical  
506 cyclone count, which is sensitive to model resolution (Roberts et al., 2020a).

507

508 Recent analysis of an ensemble of HadGEM3-GC3.1 simulations, performed under  
509 HighResMIP, demonstrated that mean skill in representing interannual variability in tropical  
510 cyclone count improves with additional members (Roberts et al., 2020a). At present, the  
511 required six-hourly geopotential outputs are available for too few ensemble members to  
512 repeat such an analysis for tropical cyclones undergoing ET, but this would constitute  
513 valuable future work when sufficient model output is obtainable. Nonetheless, quantifying  
514 the level of skill that exists in capturing interannual variability in the subset of tropical  
515 cyclones that undergo ET, while lower than that for all tropical cyclones, is important,  
516 establishing the baseline for HighResMIP-class models. This prompts further examination of  
517 ET seasonality in the historical and future atmosphere-only simulations, which is possible in  
518 the continuous PRIMAVERA simulations.

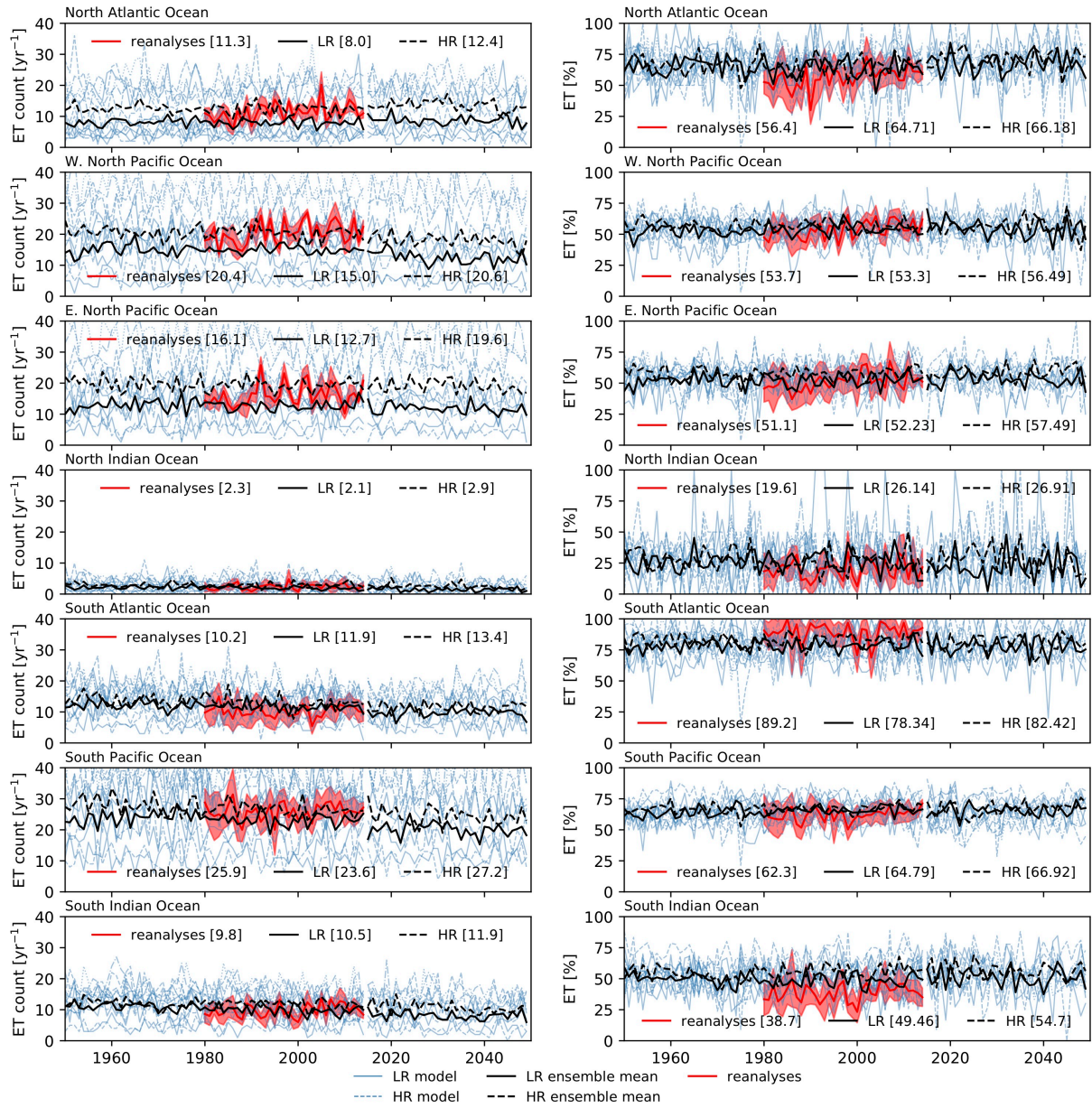
519

| Ocean basin           | ET count    |             | ET %        |             |
|-----------------------|-------------|-------------|-------------|-------------|
|                       | LR          | HR          | LR          | HR          |
| North Atlantic        | <b>0.31</b> | <b>0.30</b> | 0.24        | -0.16       |
| Western North Pacific | <b>0.50</b> | <b>0.34</b> | 0.21        | 0.24        |
| Eastern North Pacific | <b>0.43</b> | 0.22        | <b>0.42</b> | 0.16        |
| North Indian          | -0.08       | 0.03        | 0.03        | <b>0.38</b> |
| South Atlantic        | 0.07        | <b>0.34</b> | 0.12        | 0.27        |
| South Pacific         | 0.08        | <b>0.50</b> | 0.17        | <b>0.34</b> |
| South Indian          | -0.04       | -0.19       | 0.24        | <b>0.33</b> |

520

521 **Table 4.** Pearson’s  $r$  coefficients for correlations between low- (LR) or high-resolution (HR)  
522 ensemble-mean and multireanalysis-mean interannual variability in ET count and ET % for  
523 each ocean basin. Coefficients are shown only for *highresSST-present*; *hist-1950* simulations  
524 are not shown because it is not expected that coupled models’ internal year-to-year variability  
525 would mimic that of forced simulations or reanalyses. Significant ( $p < 0.1$ ) correlations are in  
526 bold type.

527



528

529 **Fig. 4.** As in Fig. 3 for fully coupled *hist-1950* and *highres-future* simulations.

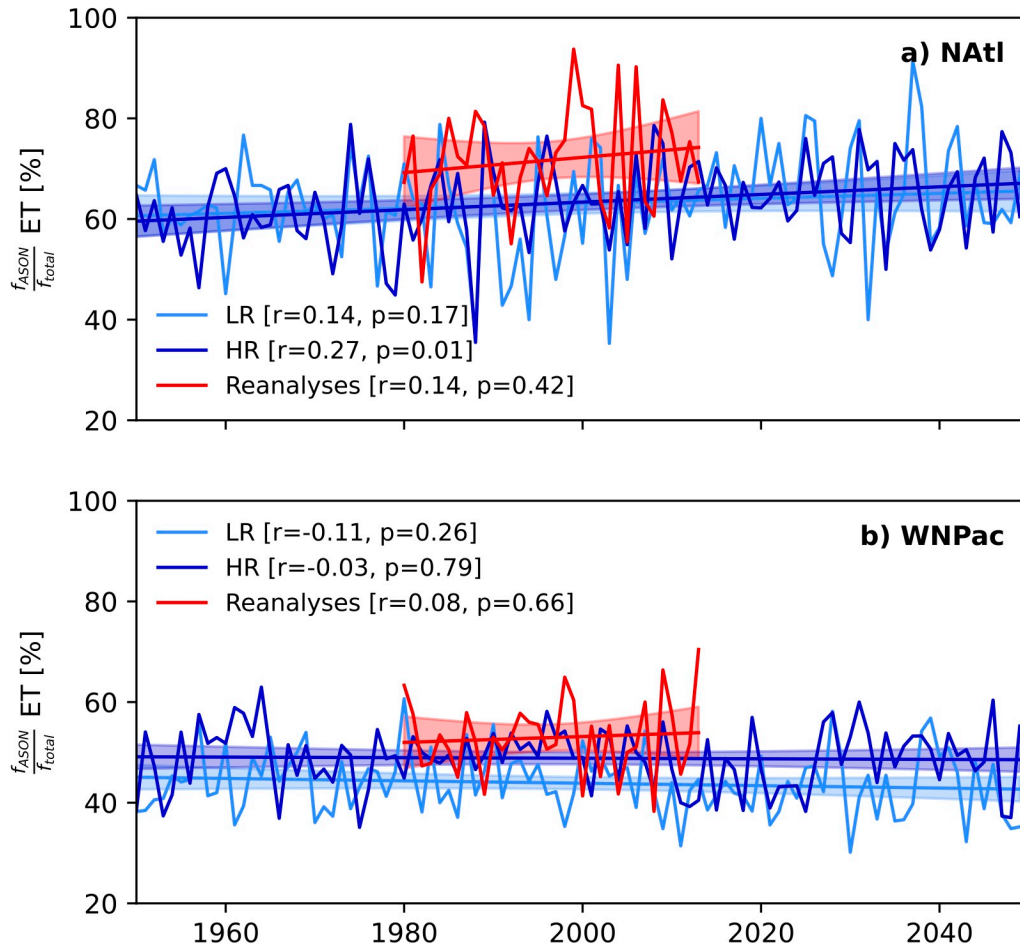
530

531 *3.3 Historical and future ET seasonality*

532 We next evaluate the seasonal cycle of ET, focussing on the North Atlantic and Western  
533 North Pacific basins for which both climatological ET statistics (Fig. 1) and interannual ET  
534 variability (Table 4) are represented reasonably across models. In the North Atlantic,  
535 reanalyses show ET % increasing from July to a peak in September before declining into  
536 winter (Fig. S6a). In the *highresSST-present* experiment, most models reproduce this  
537 seasonality, but the magnitude of the seasonal peak is overestimated by ~10 % at high-  
538 resolution. There are indications that increased atmospheric resolution improves the  
539 simulation of the timing of the seasonal ET % peak. Two models—CNRM-CM6.1 and EC-  
540 Earth3P—simulate the seasonal peak too early (in August) at low resolution but simulate a  
541 later peak (in September) at high resolution. Additionally, MPI-ESM1.2, the lowest-  
542 resolution model in this ensemble, simulates comparably muted seasonality that also peaks  
543 earlier than reanalyses at both resolutions. In the fully coupled *hist-1950* experiment, models  
544 reproduce the multireanalysis-mean seasonal cycle, but HadGEM3-GC3.1 and CNRM-  
545 CM6.1 simulate a broader seasonal distribution compared with reanalyses (Fig. S7a). In the  
546 Western North Pacific, reanalyses show bimodal seasonality, with peaks in ET % in May and  
547 September (Fig. S6b). Excepting the MPI-ESM1.2 model, which does not capture  
548 bimodality, *highresSST-present* simulations also exhibit two seasonal peaks, but each occurs  
549 one to two months later than in reanalyses in both low- and high-resolution integrations (Fig.  
550 S6b), and this also holds true for *hist-1950* simulations (Fig. S7b).

551

552 To assess any potential future change in seasonality,  $\Delta ET$  %, we differenced the historical  
553 and future seasonal cycles. For the North Atlantic, despite pronounced inter-model spread  
554 throughout most of the annual cycle, there is an indication of more consistent model  
555 behaviour during August–November, months for which most models simulate an increase in  
556 ET % in both the *highresSST-future* (Fig. S6c) and *highres-future* experiments (Fig. S7c). To  
557 quantify the degree to which this inter-model consistency represents secular change in ET  
558 seasonality, the annual fraction of total annual ET events occurring during August–November  
559 was computed. A significant, positive trend in this quantity over the period 1950–2050 is  
560 found in the ensemble mean of high-resolution atmosphere-only simulations (Fig. 5a), but the  
561 trend is not significant in reanalyses, which likely cover too short a period (1980–) to assess  
562 secular change, and is significant in the low-resolution ensemble mean only at the 80 % level.  
563 In fully coupled simulations, no significant trends are seen (Fig. S8a). Conducting a similar  
564 analysis of the forthcoming extension of ERA5 back to 1950 is warranted, pre-satellite  
565 observational uncertainty notwithstanding. For the Western North Pacific, the inter-model  
566 spread during the annual cycle of  $\Delta ET$  % is similar between *highresSST-future* (Fig. S6d) and  
567 *highres-future* simulations (Fig. S7d) and, in contrast to the North Atlantic, no significant  
568 secular change in ET seasonality is found in either reanalyses or in PRIMAVERA  
569 simulations out to 2050 (Fig. 5b and Fig. S8b). However, together with projected changes in  
570 track density (Fig. 2a–b, d–e), these results provide further evidence that the future response  
571 of ET to climate change across the North Atlantic differs from that of the Western North  
572 Pacific and of other ocean basins. Therefore, we next investigate the role of cyclone structure  
573 in explaining these distinct North Atlantic and Western North Pacific responses.  
574



575

576 **Fig. 5.** Secular change in the proportion of ET events occurring during August–November in  
 577 reanalyses (red) and low- (pale blue) and high-resolution (dark blue) atmosphere-only  
 578 simulations (ensemble mean) for the (a) North Atlantic and (b) Western North Pacific basins.  
 579 Shading shows the 95 % confidence interval for the linear fit. ECMWF-IFS is not included in  
 580 this analysis because no future simulations were performed in HighResMIP for this model.

581



### 582 3.4 Response of cyclone structures to climate change

583 To examine the response of cyclone core structure to climate change, we computed  
584 ensemble-mean bivariate frequency distributions of phase-space parameters,  $B$ ,  $T_L$ , and  $T_U$  in  
585 the high-resolution simulations. The  $T_L$ – $B$  distribution exhibits a similar general structure in  
586 the *highresSST-present* and *-future* experiments for both the North Atlantic (Fig. 6a–b) and  
587 Western North Pacific (Fig. 6d–e) basins. This is also true for  $T_L$ – $T_U$  distributions (Fig. 7a–b  
588 and Fig. 7d–e). Generally, tropical cyclones undergoing ET occupy the lower-right  
589 (symmetric, warm core) and upper-left (asymmetric, cold core) quadrants, with fewer  
590 instances in either hybrid (transitional) quadrant. The phase-space parameter distributions  
591 simulated across PRIMAVERA models are consistent with previous studies (Hart et al.,  
592 2006; Michaelis and Lackmann, 2019). Historical ensemble-mean values of  $B$  and  $T_L$  for the  
593 North Atlantic are consistent with recent analysis of observations (Studholme et al., 2015) as  
594 well as reanalyses and Community Atmosphere Model simulations at resolutions of 55 and  
595 28 km (Zarzycki et al., 2017). Ensemble-mean  $T_U$  values are also consistent with these  
596 existing studies, except that deep warm-core structures are less frequent in PRIMAVERA  
597 models than in recent 15-km-resolution simulations with the Model for Prediction Across  
598 Scales–Atmosphere model (Michaelis and Lackmann, 2019), likely due to differences in  
599 atmospheric resolution. For the Western North Pacific, model-simulated phase-space  
600 parameters are consistent with reanalysis-based values (Kitabatake, 2011). In the fully  
601 coupled simulations,  $T_L$ – $B$  distributions for both basins are similar to those of the  
602 atmosphere-only simulations (Fig. 8c, f), but differences in ensemble-mean  $T_U$  values are  
603 seen, with warm-core responses to climate change occurring variously throughout the  
604 troposphere (Fig. 9c, f).

605

606 Under climate change, models forced by prescribed SST simulate stronger warm-core  
607 structures in the North Atlantic, indicated by a shift towards higher  $T_L$  for axisymmetric  
608 tropical cyclones (Fig. 6c). Moreover,  $T_L$ – $T_U$  distributions show that the future shift to  
609 stronger warm-core structures is primarily confined to the lower troposphere (Fig. 7c, f).  
610 (Here, ‘strong’ refers to ensemble-mean  $T_L$  values at the higher end of the historical  
611 distributions, in which a range of model-simulated intensities are averaged.) These findings  
612 are supported by a recent single-model study (Michaelis and Lackmann, 2019), albeit the  
613 ensemble-mean signal we report is less pronounced, and are consistent with increased low-  
614 level moisture and the potential for enhanced latent heat release in a warmer climate. Future  
615 changes in core structures offer a partly mechanistic explanation of the projected increase in

616 ET across the North Atlantic (Baatsen et al., 2015; Haarsma et al., 2013; Liu et al., 2017) as  
617 well as the projected change in track density, which is largely unique to the North Atlantic  
618 (Fig. 2a–b, d–e). The lesser energy of weak warm-core cyclones is more likely to dissipate  
619 before ET may occur, but relatively strong warm-core structures make cyclones more  
620 resilient to unfavourable midlatitude environmental conditions (primarily cooler SST and  
621 increased vertical wind shear), prolonging their poleward propagation and making ET more  
622 probable across the North Atlantic (Hart et al., 2006).

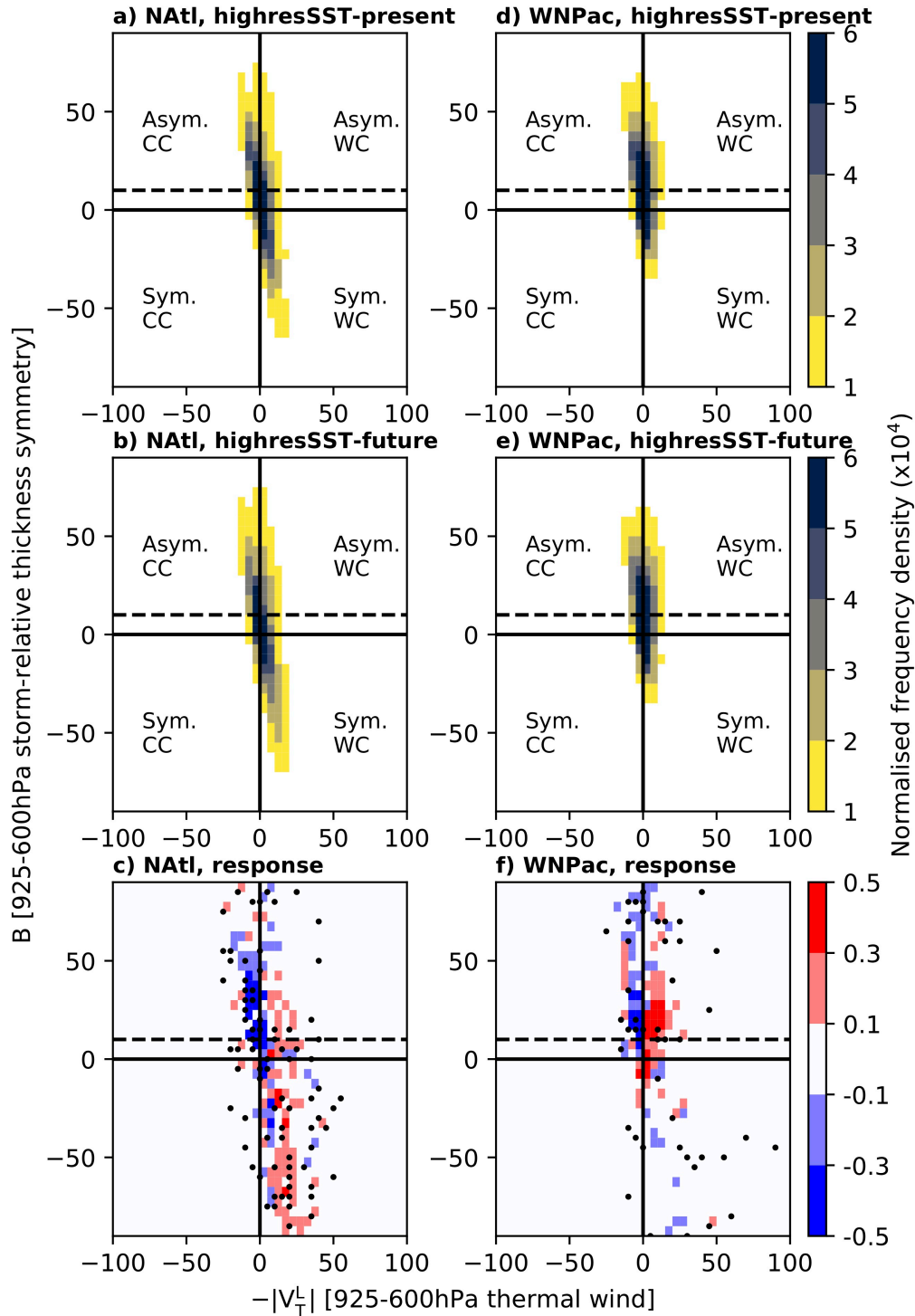
623

624 In the North Pacific, however, this future shift to stronger warm cores is not seen in  
625 PRIMAVERA models (Fig. 6f), although more frequent asymmetric, warm-core hybrid  
626 structures (upper-right quadrant) in the future are simulated. These instances of hybrid  
627 structures show cyclones existing more frequently in the transitional quadrants, potentially  
628 indicating a future elongation of ET time (Zarzycki et al., 2017) and an increase in warm-  
629 seclusion occurrences, which involve multiple transitions (Baker et al., 2021; Dekker et al.,  
630 2018). Also seen is a shift towards stronger upper-level, cold-core structures (Fig. 7f). The  
631 Western North Pacific is therefore characterised by more mixed future changes in core-  
632 structure frequencies, consistent with the projected response of track density, which generally  
633 decreases across the basin but increases in localised areas (Fig. 2b, e). Broadly, these results  
634 are also consistent with the lack of any consensus in published projections of ET frequency  
635 across the Western North Pacific: both a less favourable future ET environment (Ito et al.,  
636 2016) versus moderate future increase in ET frequency (Bieli et al., 2020) have been  
637 suggested. For both basins, future phase-space changes in the fully coupled simulations  
638 resemble those seen in the atmosphere-only experiments, but the North Atlantic climate-  
639 change signal is comparably muted (Fig. 8c, f; Fig. 9c, f).

640

641 Overall, these results help clarify the potential role that the climate-change response of  
642 cyclones' core structures have in determining future ET frequency changes, and quantifies  
643 how this differs between basins. Differences in pre-ET structures potentially underpin basin-  
644 specific responses of ET to climate change, and consistency exists among PRIMAVERA  
645 models. However, to fully explain what drives disparate North Atlantic and Western North  
646 Pacific responses, further studies of future changes in cyclogenesis and midlatitude large-  
647 scale conditions are needed, based on models of higher resolution than those in  
648 PRIMAVERA, which better simulate the most intense systems (Judt et al., 2021), and,  
649 potentially, their interactions with the large-scale environment.





651

652

653

654

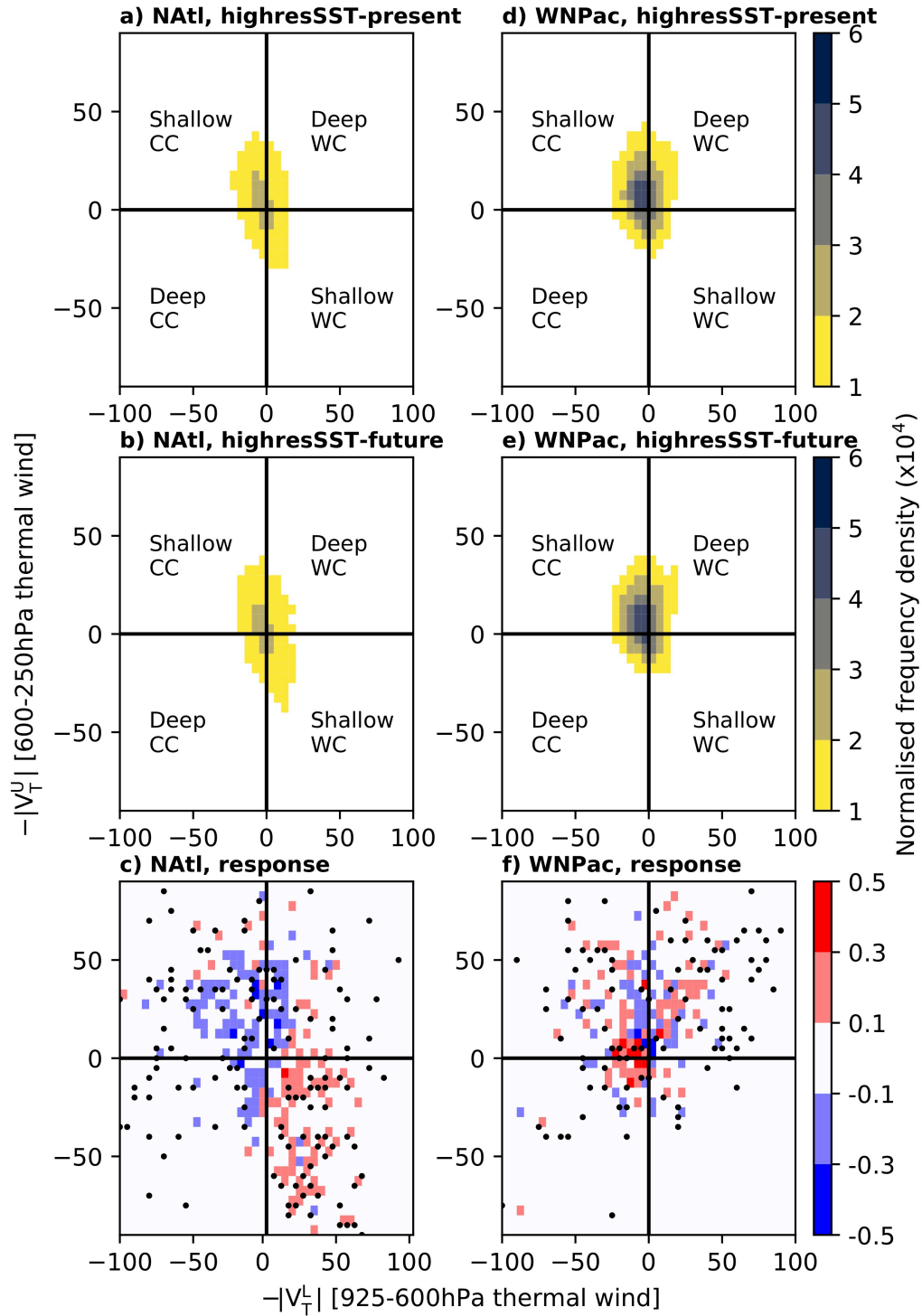
655

656

657

**Fig. 6.** Ensemble-mean distributions of  $T_L$  versus  $B$  in high-resolution (a, d) *highresSST-present* and (b, e) *-future* simulations as well as (c, f) the climate-change response for the North Atlantic ('NAtl') and Western North Pacific ('WNPac'). Distributions are computed from every 6-hourly point during the entire lifetime of all storms undergoing ET, plotted as two-dimensional histograms, and normalised by the total number of cyclones (sample sizes for each model are given in Table 3). Values are scaled by  $10^4$ . Cyclone phase-space

658 categories are warm- ('WC') or cold-core ('CC') and either symmetrical (i.e., non-frontal;  
659 'Sym.') or asymmetrical (i.e., frontal; 'Asym.'). The threshold of 10 m used to distinguish  
660 thermally symmetric from asymmetric cyclones is indicated (dashed line). Stippling in c) and  
661 f) indicates where all models agree on the sign of the difference.  
662



663

664

665

666

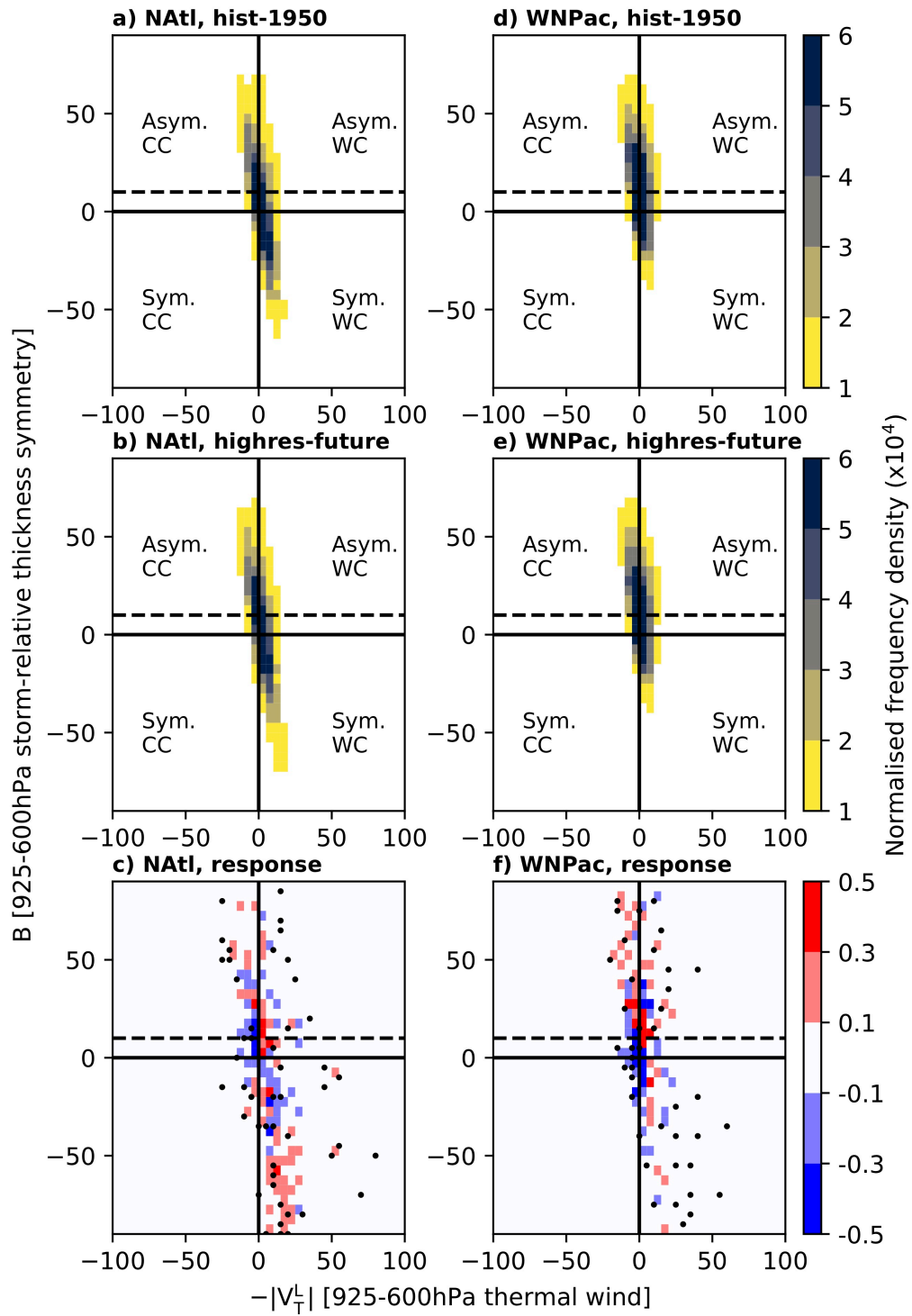
667

668

669

**Fig. 7.** Ensemble-mean distributions of  $T_L$  versus  $T_U$  in high-resolution (a, d) *highresSST-present* and (b, e) *-future* simulations as well as (c, f) the climate-change response for the North Atlantic ('NAtl') and Western North Pacific ('WNPac'). Distributions are computed from every 6-hourly point during the entire lifetime of all storms undergoing ET, plotted as two-dimensional histograms, and normalised by the total number of cyclones (sample sizes for each model are given in Table 3). Values are scaled by  $10^4$ . Cyclone phase-space

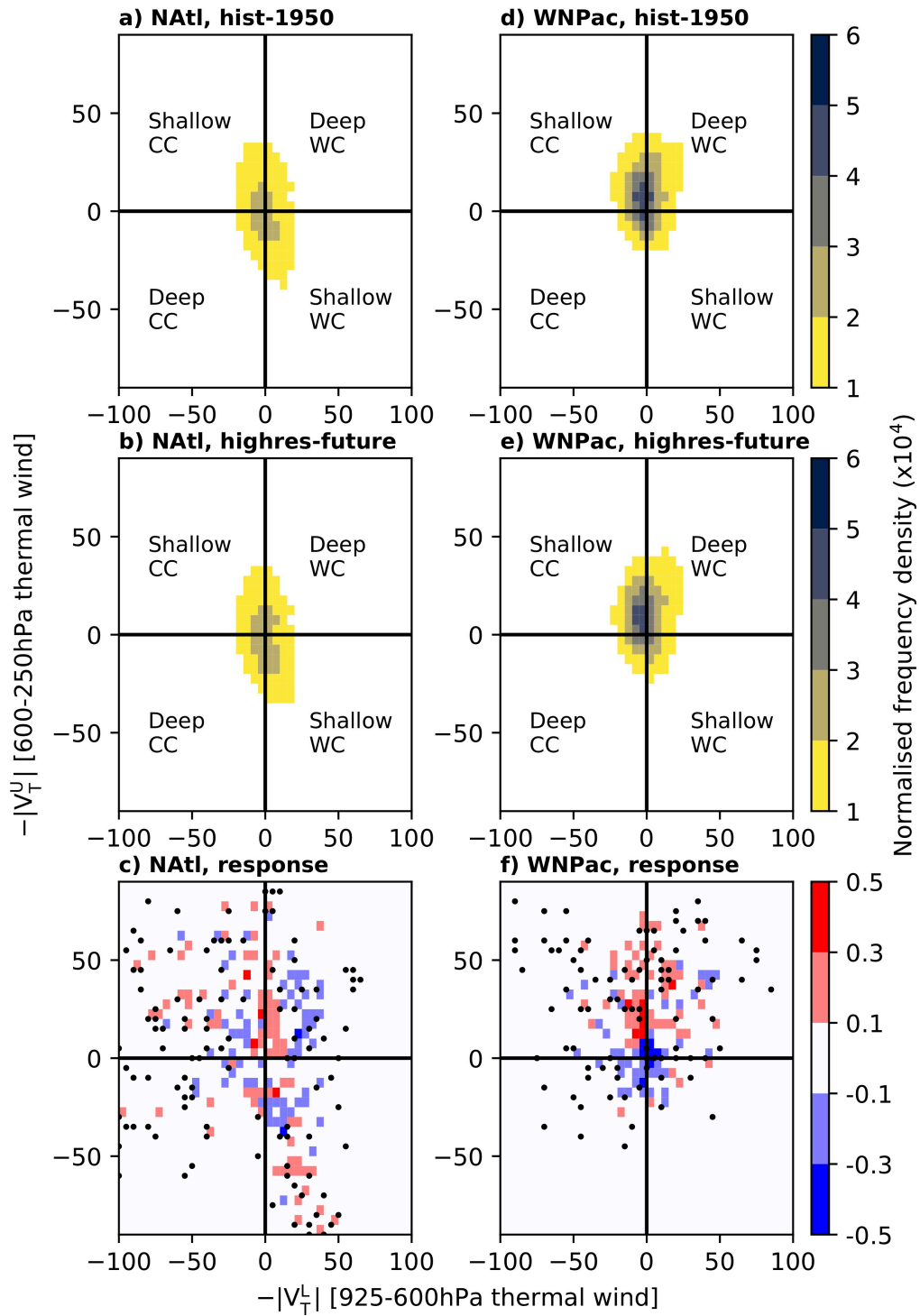
670 categories are shallow or deep warm- ('WC') or cold-core ('CC'). Stippling in c) and f)  
671 indicates where all models agree on the sign of the difference.  
672



673

674 **Fig. 8.** As in Fig. 6 for *hist-1950* and *highres-future* experiments.





675

676 **Fig. 9.** As in Fig. 7 for *hist-1950* and *highres-future* experiments.

677

678 *3.5 Pre- and post-ET cyclone intensity*

679 During ET, cyclones develop low-level frontal structures and their horizontal size increases  
680 (Evans et al., 2017). As such, increasing model resolution is expected to impact the  
681 simulation of cyclones pre- and post-ET differently, particularly in models whose effective  
682 resolutions coarsen equatorward. However, performing a global analysis of the pre- and post-  
683 ET stages of tropical cyclones' lifecycles is not trivial because ET pathways (i.e., the order in  
684 which  $B$  and  $T_L$  changes occur) differ between ocean basins (Bieli et al., 2019). We therefore  
685 separated cyclone tracks' warm- and cold-core stages about ET completion, when both  $B$  and  
686  $T_L$  satisfy ET criteria, following the definition first used by Hart (2003). Our additional 1-day  
687 criterion (see Methods) helps increase confidence in the following inter-model comparison.

688

689 Compared with best-track intensity estimates, certain atmosphere-only models (particularly  
690 CNRM-CM6.1) simulate realistic intensities at resolutions in the range 20–50 km (Roberts et  
691 al., 2020a). However, best-track intensity estimates are not well suited to evaluating post-ET  
692 systems (Velden et al., 2006), and the available primary cyclone wind-speed observations,  
693 such as satellite scatterometry data, seldom include cyclones' post-tropical stages and span  
694 too short a temporal range for climatological evaluation. We therefore turn to reanalyses,  
695 which are constrained by observational data, to provide a homogeneous global reference. An  
696 important caveat, however, is the underestimation of cyclone wind speeds in reanalyses  
697 (Hodges et al., 2017; Murakami, 2014), although this underestimation is less marked at  
698 higher latitudes (Sainsbury et al., 2020).

699

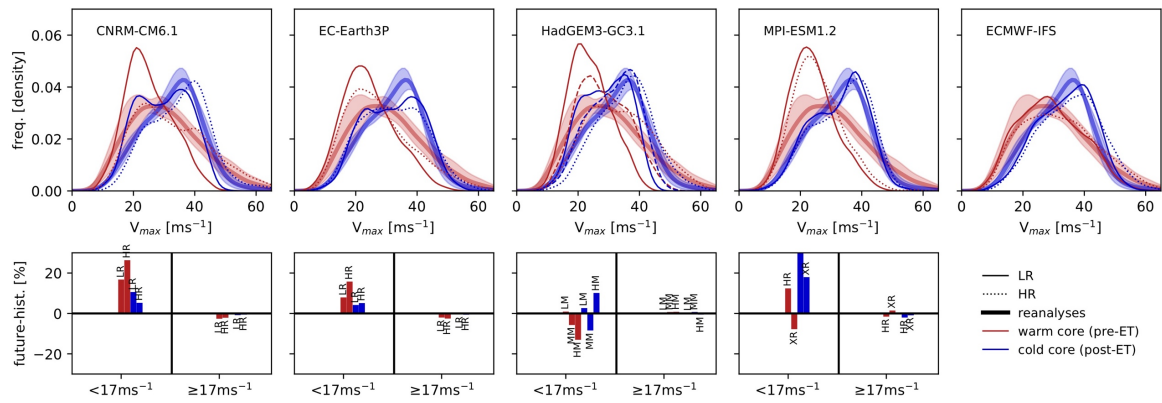
700 Considering all storms globally, PRIMAVERA models reproduce the reanalyses' cold-core,  
701 post-ET intensity distributions at both low and high resolution and in both atmosphere-only  
702 and fully coupled simulations (Fig. 10 and Fig. 11, top rows). However, models'  
703 representation of warm-core, pre-ET distributions improve markedly with increasing  
704 resolution, especially for CNRM-CM6.1 and HadGEM3-GC3.1, but more clearly so in the  
705 atmosphere-only than in the fully coupled simulations, wherein cold-wake feedbacks reduce  
706 upper-ocean temperatures and weaken subsequent tropical cyclones (Balaguru et al., 2014).  
707 Sensitivity to resolution is similar in the fully coupled CNRM-CM6.1 and HadGEM3-GC3.1  
708 simulations (Fig. 11, top row). These results show that horizontal resolutions typical of  
709 CMIP6 appear sufficient to simulate cold-core (post-ET) intensity distributions, including the  
710 relatively high-intensity tail—resolutions at which large-ensemble studies to quantify  
711 multiannual variability of the strongest post-ET storms are computationally feasible.

712 However, among high-resolution PRIMAVERA models, the high-intensity tail of the warm-  
713 core distribution is reproduced only by CNRM-CM6.1.

714

715 For *highresSST-future*, several models project decreasing warm-core and increasing cold-  
716 core intensities for weaker storms ( $<17\text{ms}^{-1}$ ) but simulate opposite warm- and cold-core  
717 responses for stronger storms ( $\geq 17\text{ms}^{-1}$ ) (Fig. 10, bottom row). This warm-core response is  
718 consistent with projections of intensified tropical cyclones under anthropogenic warming  
719 (Knutson et al., 2020). However, these responses are not replicated by fully coupled models  
720 (Fig. 11, bottom row), in which intensity changes are weak (Roberts et al., 2020b). In the  
721 fully coupled simulations, the responses of pre- and post-ET intensity distributions to climate  
722 change are equivocal, with substantial inter-model differences. We speculate that the climate-  
723 change forcing out to 2050 in the HighResMIP experimental protocol is insufficiently strong  
724 (i.e., the future simulation period is too short) for a clear signal to emerge. However, it is  
725 unclear whether intensity changes would be seen. For tropical cyclones overall, Roberts et al.  
726 (2020b) found a weak future intensification in these simulations, and Bieli et al. (2020) found  
727 equivocal ET climate-change responses in many basins out to 2100 under the weaker RCP4.5  
728 scenario. If a clear climate-change signal were to emerge with further increases in model  
729 resolution, which would increase the relative difference between the weakest and strongest  
730 simulated tropical cyclones, this would suggest that processes important for intensity change  
731 are not adequately captured at  $\sim 25$  km resolution.

732



733

734

735

736

737

738

739

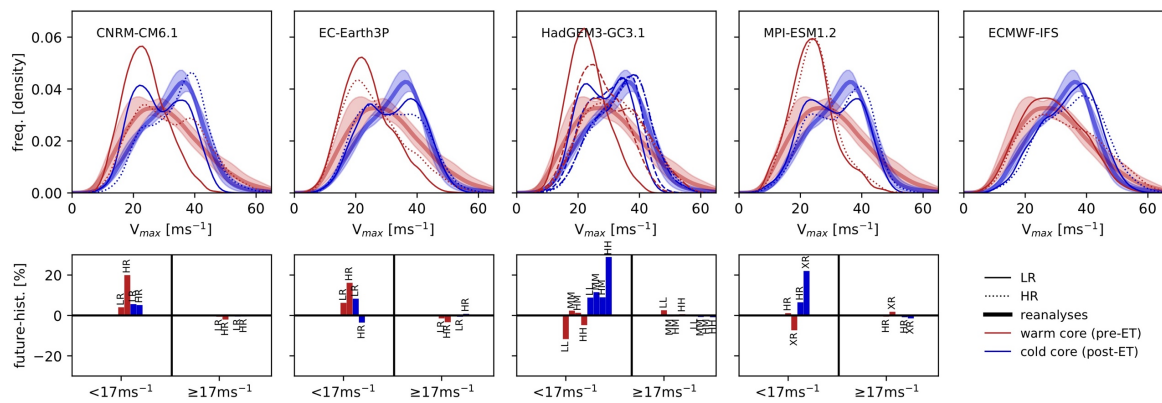
740

741

742

743

**Fig. 10.** Intensity ( $v_{max}$  at 925hPa) distributions in atmosphere-only simulations for all cyclones undergoing ET globally. For each model, historical simulations are shown in the top row and future simulations in the bottom row. Multireanalysis-mean curves (thick, solid lines) are shown with 1 s.d. (shading). Both low- (thin, solid lines) and high-resolution (thin, dashed lines) simulations are shown. Climate-change responses (i.e., *highresSST-future* minus *highresSST-present*), computed as integrated differences, are shown as percentages for storms whose lifetime-maximum intensity is  $<17 \text{ ms}^{-1}$  or  $\geq 17 \text{ ms}^{-1}$  for each atmospheric model resolution (ordered left to right).



744

745

746

**Fig. 11.** As in Fig. 10 for fully coupled simulations.

### 747 3.6 Post-ET reintensification

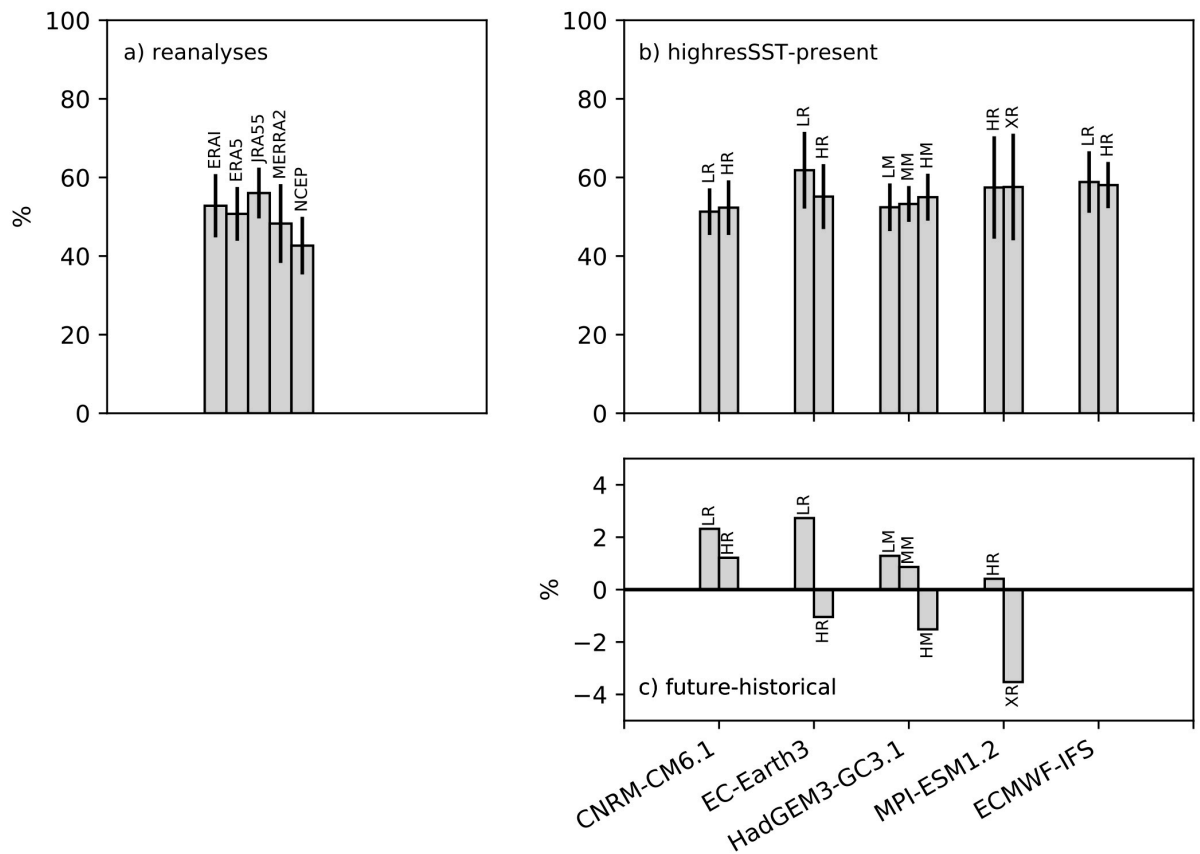
748 The lifetime-maximum intensity of transitioning tropical cyclones typically occurs during the  
749 warm-core, tropical phase. However, the addition of a baroclinic energy source and cyclone-  
750 wave interactions induce post-ET reintensification (Evans et al., 2017). We quantified the  
751 frequencies of reintensifying versus non-reintensifying cyclones in reanalyses and in the  
752 PRIMAVERA ensemble. Globally, reanalyses indicate that approximately 50 % of tropical  
753 cyclones that undergo ET undergo post-ET reintensification (Fig. 12a). For the North  
754 Atlantic and Western North Pacific basins, ~55 and ~45 %, respectively, reintensify (not  
755 shown), consistent with Hart and Evans (2001). These results are not significantly different  
756 when reintensification is defined using 925-hPa wind speed (not shown). Globally,  
757 PRIMAVERA models generally overestimate climatological reintensification frequency at  
758 low resolution, but increasing resolution decreases the proportion of reintensifying systems  
759 (and increases the proportion of non-reintensifying systems) in all models except MPI-  
760 ESM1.2, which better matches reanalyses (Fig. 12b and Fig. 13b). This result potentially  
761 reflects improved simulation of the interactions between cyclones and the large-scale  
762 circulation, which acts to reintensify systems (Keller et al., 2019), at high resolution. Which  
763 processes facilitate such improvement should be a focus of future research because these  
764 processes will be important for risk assessments of reintensification. However, it is also  
765 possible that post-ET reintensification arises in models whose effective resolution increases  
766 with increasing latitude (e.g., HadGEM3-GC3.1), allowing stronger simulated winds at  
767 higher latitudes, but the impact of this artifact will be reduced at higher resolutions.

768

769 In HadGEM3-GC3.1, for an atmospheric resolution of 25 km (at 50 ° latitude), increasing  
770 ocean resolution from 1/4 ° to 1/12 ° (-HM and -HH, respectively) does not impact the  
771 proportion of reintensifying cyclones (Fig. 13b). An increase in the proportion might be  
772 expected because increasing ocean resolution and therefore more sharply resolving SST  
773 fronts (around western boundary currents; Fig. S5) is likely to enhance baroclinicity and  
774 provide atmospheric conditions conducive to post-ET reintensification. That no increase is  
775 seen implies that atmospheric resolution, to which simulated tropical-cyclone frequency and  
776 intensity are sensitive, acts as a constraint on reintensification statistics, at least for this  
777 particular model. Further investigation with multiple ocean models would establish more  
778 robustly whether this is the case.

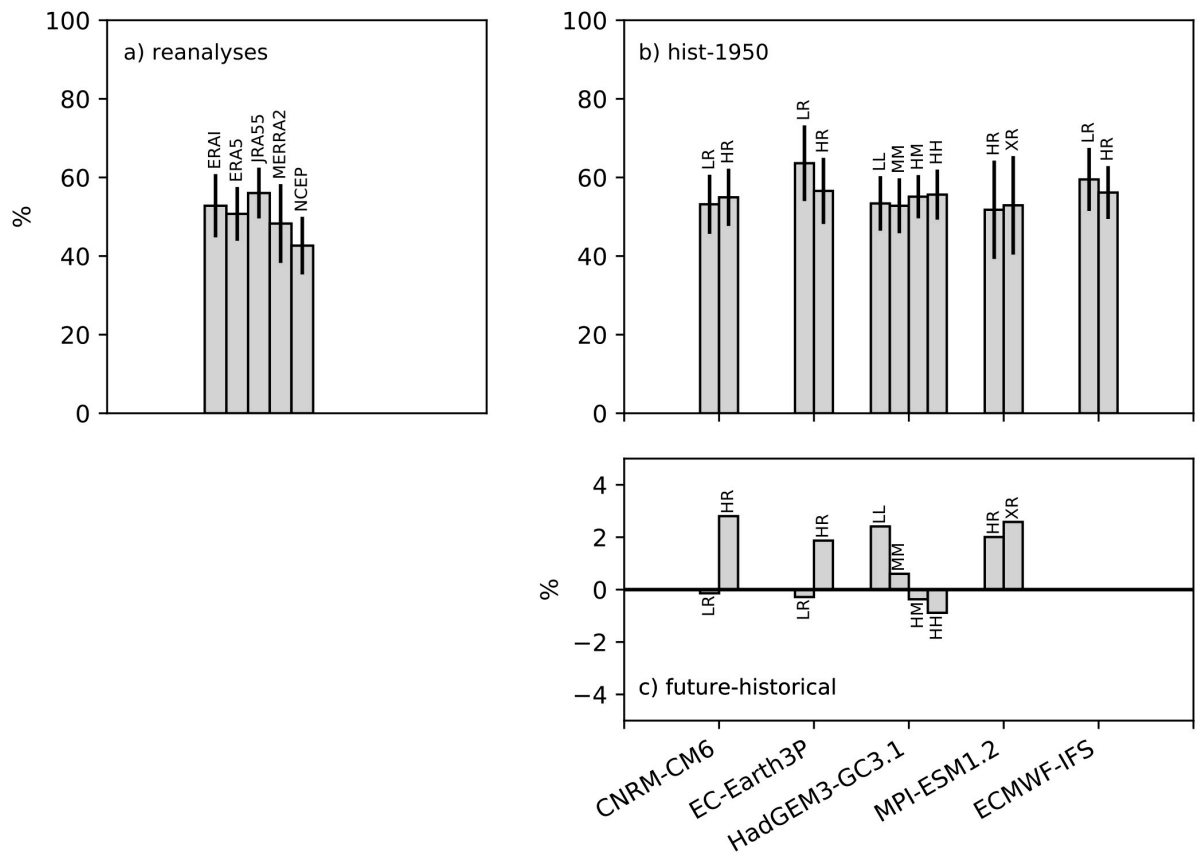
779

780 In both the atmosphere-only and fully coupled simulations, future changes in the proportion  
781 of post-ET reintensifying systems are small and generally within one standard deviation of  
782 historical interannual variability (Fig. 12c and Fig. 13c), again suggesting that any climate-  
783 change response under RCP8.5 emerges after 2050. In atmosphere-only simulations, low-  
784 resolution models all simulate an increase the proportion of reintensifying cyclones, but high-  
785 resolution models simulate a decrease (Fig. 12c), except for CNRM-CM6.1. Fully coupled  
786 models typically simulate a future increase across resolutions (Fig. 13c).  
787



788  
 789  
 790  
 791  
 792  
 793  
 794

**Fig. 12.** Global analysis of the percentage of transitioning storms that undergo post-ET reintensification in (a) reanalyses and (b) *highresSST-present* simulations, and (c) the percentage change simulated for *highresSST-future* experiments. One standard deviation of interannual variability is indicated for each reanalysis and historical model simulation (black lines).



795

796 **Fig. 13.** As Fig. 12 but for *hist-1950* and *highres-future* simulations.

797



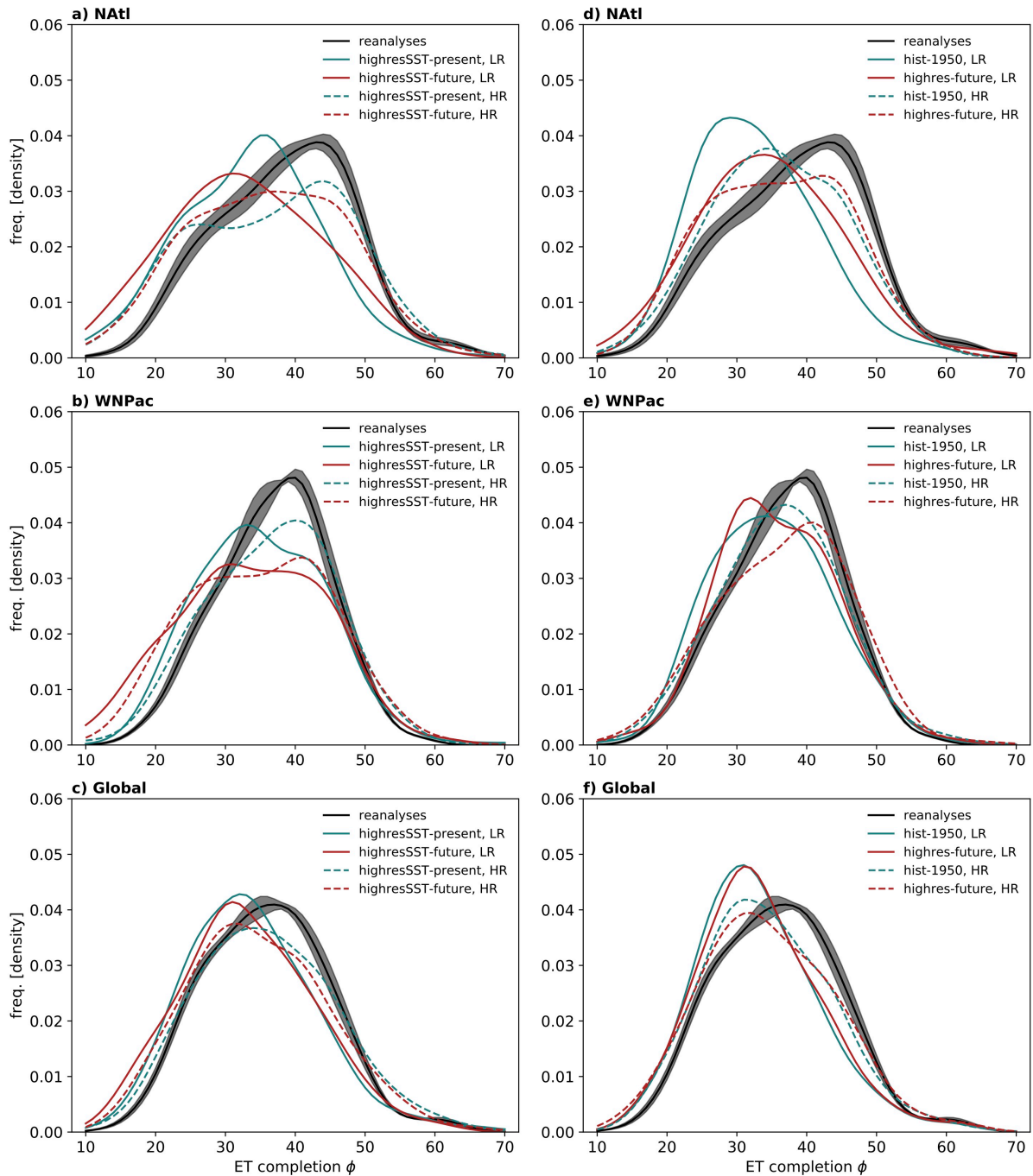
798 3.7 ET latitude

799 Finally, we assess how ET location responds to both increased resolution and to climate  
800 change out to 2050. Distributions of ET-completion latitude were computed from reanalyses  
801 and all PRIMAVERA experiments globally as well as well as separately for the basins where  
802 models exhibit the best performance: the North Atlantic and Western North Pacific basins  
803 (Fig. 14). For *highresSST-present*, model-simulated ET completion occurs at lower latitudes  
804 than in reanalyses (Fig. 14a–c). At high resolution, this is partially rectified: peak frequency  
805 occurs at a similar latitude to reanalyses in both the North Atlantic (Fig. 14a) and Western  
806 North Pacific (Fig. 14b), but the magnitudes of both peaks are underestimated and  
807 occurrences of low-latitude ET (i.e., 10–20 °) remain too frequent. Globally, an equatorward  
808 bias in peak frequency across resolutions indicates that ET-completion latitude is less well  
809 simulated in other basins (Fig. 14c). These results hold true for *hist-1950* simulations (Fig.  
810 14d–f), except there are fewer instances of low-latitude ET (i.e., 10–20 °), likely reflecting  
811 slower development of warm-core structures and subsequent ET in the fully coupled  
812 experiments.

813

814 In response to climate change, the ensemble-mean distribution of ET-completion latitude  
815 exhibits an equatorward shift in the North Atlantic in the atmosphere-only experiment (Fig.  
816 14a), but a poleward shift in the fully coupled simulations (Fig. 14d), with an increased  
817 frequency of ET completion particularly between 45–55 °N. In the Western North Pacific, a  
818 poleward shift is seen in the latitude of the peak frequency, from ~30 to ~40 °N, in both  
819 experiments, but little change is simulated at higher latitudes (i.e., > 45 °N). Globally, a small  
820 equatorward shift of ~2 ° is simulated in atmosphere-only (Fig. 14c) and no meridional shift  
821 is seen in coupled simulations (Fig. 14f). Previously, we showed stronger low-level warm-  
822 core structures are simulated in future (Fig. 6 and Fig. 8), which potentially allow tropical  
823 cyclones to propagate farther poleward prior to ET, with the most pronounced signal seen in  
824 the North Atlantic. While coupled PRIMAVERA models provide evidence for a poleward  
825 shift of ET, climate-change responses globally are equivocal out to 2050.

826



827

828

829

830

831

832

833

834

835

**Fig. 14.** Ensemble-mean frequency distributions of ET-completion latitude for (solid lines) low- and (dashed lines) high-resolution simulations, for both 1950–2014 (teal) and 2015–2050 (red). Results are shown for (a–c) atmosphere-only and (d–f) fully coupled experiments for the North Atlantic basin (“NATl”), Western North Pacific basin (“WNPac”) and all global basins combined. ‘LR’ and ‘HR’ denote low- and high-resolution distributions, respectively. Also shown is the multireanalysis-mean distribution with shading indicating the standard error for the five reanalyses. Note that frequency is plotted as a function of absolute latitude ( $\phi$ ) to combine Northern and Southern Hemisphere results in c) and f).

836

#### 837 **4. Summary and discussion**

838 This paper presents an analysis of ET across five reanalysis datasets and climate simulations  
839 performed with five atmosphere-only and full coupled global models participating in CMIP6  
840 HighResMIP, focussing on (i) the effect of increased model resolution on the representation  
841 of ET and (ii) the response of ET to climate change.

842

843 For all tropical cyclones undergoing ET, we find an increase in the climatological track  
844 density simulated at high resolution (~25 km) compared with low resolution (~100 km) in all  
845 ocean basins and in both atmosphere-only and fully coupled model configurations (Fig. 1b,  
846 d), particularly over Northern Hemisphere western boundary currents. Model error in  
847 simulated track density (compared with the multireanalysis-mean track density) is reduced at  
848 high resolution in the North Atlantic and Western North Pacific (Fig. 1c, e). The simulated  
849 climatological annual-mean count of ET events is closer to that of reanalyses in the ocean  
850 basins where ET activity is highest—the North Atlantic and the Western and Eastern North  
851 Pacific—in both atmosphere-only (Fig. 3) and fully coupled (Fig. 4) experiments. In these  
852 basins, atmosphere-only simulations exhibit skill of ~0.3 in capturing interannual variability  
853 in just the subset of tropical cyclones that undergo ET (Table 4), demonstrating that the skill  
854 of these models in simulating all tropical cyclones does not remain throughout the complete  
855 cyclone lifecycle. Additionally, this level of skill in atmosphere-only simulations is lower  
856 than that found for similar-resolution initialised seasonal forecasts (Liu et al., 2018). For the  
857 other basins—the Northern Indian and Southern Hemisphere—frequencies simulated by  
858 high-resolution models overestimate reanalyses. ET %, however, is similar between low- and  
859 high-resolution simulations, indicating that the resolution sensitivity of ET is driven by that  
860 of tropical cyclone frequency, not by an enhancement of environmental conditions conducive  
861 to ET. The seasonal cycle of ET is reproduced by most models, with both the seasonal timing  
862 and the magnitude of the seasonal peak simulated more correctly at high-resolution, but the  
863 impact of increased atmospheric resolution is model-dependent.

864

865 In general, PRIMAVERA models show clearer inter-model agreement on the climate-change  
866 response of ET frequency than on the response of intensity-related metrics. For most basins,  
867 models simulate a frequency decrease in response to climate change, except over the North  
868 Atlantic, where an increase is projected (Fig. 2). The magnitude of the North Atlantic  
869 response is larger in atmosphere-only simulations than in fully coupled integrations and is

870 enhanced by increasing atmospheric model resolution, although interannual variability is  
871 pronounced (Fig. 3 and Fig. 4). A significant positive trend in the ensemble-mean fraction of  
872 North Atlantic ET events occurring during August–November is found over the period 1950–  
873 2050 at high-resolution, indicating long-term change in ET seasonality in this basin, but no  
874 secular seasonality change is simulated in the Western North Pacific (Fig. 5). North Atlantic  
875 seasonality change may result in a higher proportion of tropical cyclones encountering the  
876 midlatitude environment during the part of the seasonal cycle when, climatologically,  
877 baroclinicity is highest (Hoskins and Hodges, 2019). Opposing future ET responses between  
878 the North Atlantic and Western North Pacific are potentially underpinned by changes in low-  
879 level, pre-ET warm-core structures, which strengthen in response to climate change in the  
880 North Atlantic but undergo little change in the Western North Pacific (Fig. 6 and Fig. 7).  
881 Comparing atmosphere-only with fully coupled simulations, the North Atlantic track density  
882 response to climate change is more muted in the fully coupled experiment, which is  
883 consistent with a less pronounced climate-change response of pre-ET structures simulated by  
884 coupled models. Simulations with higher-resolution, storm-resolving models will open  
885 opportunities to further study realistically deep warm-core cyclones.

886

887 Globally, simulated warm-core, pre-ET intensity distributions improve with resolution in  
888 most models in both atmosphere-only and fully coupled experiments, better resembling  
889 reanalyses (Fig. 10 and Fig. 11). Simulated cold-core, post-ET intensity distributions exhibit  
890 little sensitivity to resolution across models. Globally, models simulate no clear climate-  
891 change response of pre- or post-ET intensity distributions, suggesting that, if a signal exists,  
892 extending simulations beyond 2050 may be required. Under *highresSST-future* forcing, some  
893 models show decreasing warm-core and increasing cold-core intensities for storms  $<17\text{ms}^{-1}$ ,  
894 but the opposite response for storms  $\geq 17\text{ms}^{-1}$ . However, this is not reproduced by fully  
895 coupled models. Globally, increasing resolution increases the proportion of simulated post-  
896 ET reintensifications to approximately match reanalyses, but not in all models. Climate-  
897 change responses are not significant with respect to historical interannual variability and are  
898 model-dependent (Fig. 12 and Fig. 13).

899

900 The role of model resolution is become clearer, but uncertainties remain. Recent analysis of  
901 tropical cyclones the PRIMAVERA simulations (Roberts et al., 2020b) has shown that the  
902 high-resolution atmosphere-only models, which typically have lower wind-speed biases,  
903 show either reduced future wind speeds or no change. Fully coupled models with the smallest

904 historical biases simulate either no change in future wind speeds or increases of only a few  
905 percent. These models therefore project weaker intensity responses to climate change  
906 compared with other studies (Knutson et al., 2020). One potential factor is the simplifying  
907 aspects of the HighResMIP protocol that are necessary to isolate the role of model resolution,  
908 particularly the standardised aerosol forcing and use of a single set of SST and sea-ice  
909 boundary conditions shared across models (Haarsma et al., 2016). For ET, the climate-change  
910 responses of pre- and post-ET intensity analysed in this study are largely model-dependent,  
911 with models exhibiting little systematic change between atmospheric resolutions of ~100 and  
912 ~25 km. This suggests that these disparate responses are due to differences in model  
913 formulation, but a larger ensemble of models is likely needed to assess this fully. For post-ET  
914 reintensification, increasing atmospheric resolution appears to result in more consistent  
915 model behaviour, but resolution remains a key research issue because several models still  
916 underestimate tropical cyclone intensities at ~25 km grid spacing (Roberts et al., 2020a) and  
917 further improvements are anticipated by increasing resolution to at least 10 km (Haarsma,  
918 2021; Judt et al., 2021). To obtain samples of ET events comparable to this study, however,  
919 running sufficiently long simulations (and / or a sufficiently large ensemble) at these storm-  
920 resolving resolutions, even without coupling to an ocean model, remains a significant  
921 computational challenge (Roberts et al., 2020b).

922

923 Additional outstanding questions and uncertainties remain. A poleward expansion of Hadley  
924 circulation termini is projected in a warmer climate (Lu et al., 2007), which implies  
925 meridional shifts in tropical storm tracks (Sharmila and Walsh, 2018; Studholme and Gulev,  
926 2018). However, the impacts of this large-scale change on the spatial distribution and  
927 frequency of ET are equivocal. The poleward expansion of regions conducive to tropical  
928 cyclone genesis and development that results from an increase in Hadley cell width will  
929 reduce the mean displacement required for tropical cyclones to reach the midlatitude  
930 baroclinic zone, increasing the likelihood of ET. However, a poleward shift of the midlatitude  
931 storm track in response to warming has been projected (Bengtsson et al., 2006), which in turn  
932 shifts environmental conditions conducive to extratropical transition poleward, potentially  
933 offsetting Hadley-driven changes. Here, we find minimal changes in ET-completion latitude  
934 out to 2050 (Fig. 14), suggesting cancellation in the net effect of these competing large-scale  
935 changes. Further work is needed to establish the time of emergence of any meridional shift  
936 and will require dedicated studies, exploring a range of climate-change scenarios with models

937 run at resolutions sufficiently high to adequately represent both tropical cyclones and ET—at  
938 least 25 km, according to our results.

939

940 This study provides evidence that pre-ET cyclone intensity and warm-core strength exert  
941 influence over future changes in ET statistics and seasonality. Analysis of higher-resolution  
942 and storm-resolving models (at least 10 km) will help establish whether these results hold  
943 true for models able to reproduce more realistic tropical-cyclone maximum intensities,  
944 including rapidly intensifying systems. Additionally, there is a need to contextualise future  
945 projections of ET, accounting for natural variability, and in particular the roles of regional  
946 (e.g., Atlantic Multidecadal Variability) and global (i.e., El Niño–Southern Oscillation)  
947 modes of variability on ET frequency. Dedicated sensitivity experiments will be required,  
948 and such a study is forthcoming for the North Atlantic, where this work has identified future  
949 changes that are important and often unique to this basin. Finally, investigation of secular  
950 change in ET seasonality, as seen in the North Atlantic in this study, will be important  
951 globally because future modification to the interval between the seasonal maximum of ET  
952 occurrence and wintertime storminess may engender considerable changes in risk for  
953 populous midlatitude regions.

954

955 **Data and code availability**

956 All reanalysis data for tropical-cyclone tracking (vorticity, wind fields, and sea-level  
957 pressure) and cyclone phase-space analysis (geopotential) are available from [rda.ucar.edu](http://rda.ucar.edu) or  
958 [disc.gsfc.nasa.gov](http://disc.gsfc.nasa.gov). Model data are available from Earth System Grid Foundation nodes  
959 ([esgf.llnl.gov](http://esgf.llnl.gov)). TRACK is available for download at [gitlab.act.reading.ac.uk/track](http://gitlab.act.reading.ac.uk/track) and the  
960 track datasets used in this paper may be downloaded from  
961 [catalogue.ceda.ac.uk/uuid/e82a62d926d7448696a2b60c1925f811](http://catalogue.ceda.ac.uk/uuid/e82a62d926d7448696a2b60c1925f811). Data analysis and  
962 visualisation code is available from the lead author upon request ([hrcm.ceda.ac.uk/contact](http://hrcm.ceda.ac.uk/contact)).

963

964 **Acknowledgements**

965 All authors received financial support from the PRIMAVERA project (European  
966 Commission Horizon2020 grant agreement 641727) with data access via JASMIN  
967 ([jasmin.ac.uk](http://jasmin.ac.uk)) supported by IS-ENES3 (grant agreement 824084). AJB also received support  
968 from National Environmental Research Council (NERC) national capability grant for the  
969 North Atlantic Climate System: Integrated study (ACSIS) program (grants NE/N018001/1,  
970 NE/N018044/1, NE/N018028/1, and NE/N018052/1). KL received funding from the German  
971 Federal Ministry of Education and Research (BMBF) through JPI Climate / JPI Oceans  
972 NextG-Climate Science-ROADMAP (FKZ: 01LP2002A). The authors are grateful to the  
973 editor and to three anonymous reviewers, whose recommendations improved this paper.

974

975 **Author contributions**

976 AJB, PLV, RJH and MJR conceived the study. Simulations were performed by MJR, ET,  
977 KL, CDR, and LT. Output data were managed by JS. MJR performed the cyclone tracking.  
978 BV computed Eady growth rate. AJB undertook cyclone phase-space analysis and all other  
979 data analyses, figure preparation, and wrote the manuscript. All authors provided input in  
980 interpreting results and approved the final manuscript.

981

982 **Competing interests**

983 The authors declare no competing interests.

984

985 **References**

- 986 Arnott, J. M., J. L. Evans, and F. Chiaromonte, 2004: Characterization of Extratropical  
987 Transition Using Cluster Analysis. *Monthly Weather Review* **132**, 2916-2937
- 988 Baatsen, M., R. J. Haarsma, A. J. Van Delden, and H. de Vries, 2015: Severe Autumn storms  
989 in future Western Europe with a warmer Atlantic Ocean. *Climate Dynamics* **45**, 949-964
- 990 Baker, A. J., K. I. Hodges, R. K. H. Schiemann, and P. L. Vidale, 2021: Historical variability  
991 and lifecycles of North Atlantic midlatitude cyclones originating in the tropics. *Journal of*  
992 *Geophysical Research: Atmospheres* **126**, e2020JD033924
- 993 Balaguru, K., S. Taraphdar, L. R. Leung, G. R. Foltz, and J. A. Knaff, 2014: Cyclone-cyclone  
994 interactions through the ocean pathway. *Geophysical Research Letters* **41**, 6855-6862
- 995 Barcikowska, M., F. Feser, and H. von Storch, 2012: Usability of Best Track Data in Climate  
996 Statistics in the Western North Pacific. *Monthly Weather Review* **140**, 2818-2830
- 997 Bengtsson, L., K. I. Hodges, and E. Roeckner, 2006: Storm Tracks and Climate Change.  
998 *Journal of Climate* **19**, 3518-3543
- 999 Bieli, M., S. J. Camargo, A. H. Sobel, J. L. Evans, and T. Hall, 2019: A Global Climatology  
1000 of Extratropical Transition. Part I: Characteristics across Basins. *Journal of Climate* **32**,  
1001 3557-3582
- 1002 Bieli, M., A. H. Sobel, S. J. Camargo, H. Murakami, and G. A. Vecchi, 2020: Application of  
1003 the Cyclone Phase Space to Extratropical Transition in a Global Climate Model. *Journal of*  
1004 *Advances in Modeling Earth Systems* **12**, e2019MS001878
- 1005 Blake, E. S., T. B. Kimberlain, R. J. Berg, C. J.P., and J. L. Beven II, 2013: Hurricane Sandy  
1006 (AL182012). *National Hurricane Center Tropical Cyclone Report*,  
1007 [https://www.nhc.noaa.gov/data/tcr/AL182012\\_Sandy.pdf](https://www.nhc.noaa.gov/data/tcr/AL182012_Sandy.pdf)
- 1008 Chang, E. K. M., and Y. Guo, 2007: Is the number of North Atlantic tropical cyclones  
1009 significantly underestimated prior to the availability of satellite observations? *Geophysical*  
1010 *Research Letters* **34**, L14801



1011 Chu, J.-H., C. R. Sampson, A. S. Levine, and E. Fukada, 2002: The Joint Typhoon Warning  
1012 Center Tropical Cyclone Best-Tracks, 1945-2000. United States Naval Research Laboratory,  
1013 NRL/MR/7540-02-16.

1014 Davis, C. A., 2018: Resolving Tropical Cyclone Intensity in Models. *Geophysical Research*  
1015 *Letters* **45**, 2082-2087

1016 Dee, D. P., S. M. Uppala, A. J. Simmons, P. Berrisford, P. Poli, S. Kobayashi, U. Andrae, M.  
1017 A. Balmaseda, G. Balsamo, P. Bauer, P. Bechtold, A. C. M. Beljaars, L. van de Berg, J.  
1018 Bidlot, N. Bormann, C. Delsol, R. Dragani, M. Fuentes, A. J. Geer, L. Haimberger, S. B.  
1019 Healy, H. Hersbach, E. V. Hólm, L. Isaksen, P. Kållberg, M. Köhler, M. Matricardi, A. P.  
1020 McNally, B. M. Monge-Sanz, J. J. Morcrette, B. K. Park, C. Peubey, P. de Rosnay, C.  
1021 Tavolato, J. N. Thépaut, and F. Vitart, 2011: The ERA-Interim reanalysis: configuration and  
1022 performance of the data assimilation system. *Quarterly Journal of the Royal Meteorological*  
1023 *Society* **137**, 553-597

1024 Dekker, M. M., R. J. Haarsma, H. d. Vries, M. Baatsen, and A. J. v. Delden, 2018:  
1025 Characteristics and development of European cyclones with tropical origin in reanalysis data.  
1026 *Climate Dynamics* **50**, 445-455

1027 Delgado, S., C. W. Landsea, and H. Willoughby, 2018: Reanalysis of the 1954–63 Atlantic  
1028 Hurricane Seasons. *Journal of Climate* **31**, 4177-4192

1029 Evans, C., K. M. Wood, S. D. Aberson, H. M. Archambault, S. M. Milrad, L. F. Bosart, K. L.  
1030 Corbosiero, C. A. Davis, J. R. D. Pinto, J. Doyle, C. Fogarty, T. J. G. Jr., C. M. Grams, K. S.  
1031 Griffin, J. Gyakum, R. E. Hart, N. Kitabatake, H. S. Lentink, R. McTaggart-Cowan, W.  
1032 Perrie, J. F. D. Quinting, C. A. Reynolds, M. Riemer, E. A. Ritchie, Y. Sun, and F. Zhang,  
1033 2017: The Extratropical Transition of Tropical Cyclones. Part I: Cyclone Evolution and  
1034 Direct Impacts. *Monthly Weather Review* **145**, 4317-4344

1035 Grams, C. M., and S. R. Blumer, 2015: European high-impact weather caused by the  
1036 downstream response to the extratropical transition of North Atlantic Hurricane Katia (2011).  
1037 *Geophysical Research Letters* **42**, 8738-8748

1038 Gutjahr, O., D. Putrasahan, K. Lohmann, J. H. Jungclaus, J. S. von Storch, N. Brüggemann,  
1039 H. Haak, and A. Stössel, 2019: Max Planck Institute Earth System Model (MPI-ESM1.2) for

1040 the High-Resolution Model Intercomparison Project (HighResMIP). *Geosci. Model Dev.* **12**,  
1041 3241-3281

1042 Haarsma, R., 2021: European Windstorm Risk of Post-Tropical Cyclones and the Impact of  
1043 Climate Change. *Geophysical Research Letters* **48**, e2020GL091483

1044 Haarsma, R., M. Acosta, R. Bakhshi, P. A. Bretonnière, L. P. Caron, M. Castrillo, S. Corti, P.  
1045 Davini, E. Exarchou, F. Fabiano, U. Fladrich, R. Fuentes Franco, J. García-Serrano, J. von  
1046 Hardenberg, T. Koenig, X. Levine, V. L. Meccia, T. van Noije, G. van den Oord, F. M.  
1047 Palmeiro, M. Rodrigo, Y. Ruprich-Robert, P. Le Sager, E. Tourigny, S. Wang, M. van Weele,  
1048 and K. Wyser, 2020: HighResMIP versions of EC-Earth: EC-Earth3P and EC-Earth3P-HR –  
1049 description, model computational performance and basic validation. *Geosci. Model Dev.* **13**,  
1050 3507-3527

1051 Haarsma, R. J., W. Hazeleger, C. Severijns, H. Vries, A. Sterl, R. Bintanja, G. J. Oldenborgh,  
1052 and H. W. Brink, 2013: More hurricanes to hit western Europe due to global warming.  
1053 *Geophysical Research Letters* **40**, 1783-1788

1054 Haarsma, R. J., M. J. Roberts, P. L. Vidale, C. A. Senior, A. Bellucci, Q. Bao, P. Chang, S.  
1055 Corti, N. S. Fučkar, V. Guemas, J. von Hardenberg, W. Hazeleger, C. Kodama, T. Koenig,  
1056 L. R. Leung, J. Lu, J. J. Luo, J. Mao, M. S. Mizieliński, R. Mizuta, P. Nobre, M. Satoh, E.  
1057 Scoccimarro, T. Semmler, J. Small, and J. S. von Storch, 2016: High Resolution Model  
1058 Intercomparison Project (HighResMIP v1.0) for CMIP6. *Geoscientific Model Development* **9**,  
1059 4185-4208

1060 Hagen, A. B., D. Strahan-Sakoskie, and C. Lueckert, 2012: A Reanalysis of the 1944–53  
1061 Atlantic Hurricane Seasons—The First Decade of Aircraft Reconnaissance. *Journal of*  
1062 *Climate* **25**, 4441-4460

1063 Harr, P. A., D. Anwender, and S. C. Jones, 2008: Predictability Associated with the  
1064 Downstream Impacts of the Extratropical Transition of Tropical Cyclones: Methodology and  
1065 a Case Study of Typhoon Nabi (2005). *Monthly Weather Review* **136**, 3205-3225

1066 Hart, R. E., 2003: A Cyclone Phase Space Derived from Thermal Wind and Thermal  
1067 Asymmetry. *Monthly Weather Review* **131**, 585-616

- 1068 Hart, R. E., and J. L. Evans, 2001: A Climatology of the Extratropical Transition of Atlantic  
1069 Tropical Cyclones. *Journal of Climate* **14**, 546-564
- 1070 Hart, R. E., J. L. Evans, and C. Evans, 2006: Synoptic Composites of the Extratropical  
1071 Transition Life Cycle of North Atlantic Tropical Cyclones: Factors Determining  
1072 Posttransition Evolution. *Monthly Weather Review* **134**, 553-578
- 1073 Hersbach, H., B. Bell, P. Berrisford, S. Hirahara, A. Horányi, J. Muñoz-Sabater, J. Nicolas,  
1074 C. Peubey, R. Radu, D. Schepers, A. Simmons, C. Soci, S. Abdalla, X. Abellan, G. Balsamo,  
1075 P. Bechtold, G. Biavati, J. Bidlot, M. Bonavita, G. De Chiara, P. Dahlgren, D. Dee, M.  
1076 Diamantakis, R. Dragani, J. Flemming, R. Forbes, M. Fuentes, A. Geer, L. Haimberger, S.  
1077 Healy, R. J. Hogan, E. Hólm, M. Janisková, S. Keeley, P. Laloyaux, P. Lopez, C. Lupu, G.  
1078 Radnoti, P. de Rosnay, I. Rozum, F. Vamborg, S. Villaume, and J.-N. Thépaut, 2020: The  
1079 ERA5 global reanalysis. *Quarterly Journal of the Royal Meteorological Society* **146**, 1999-  
1080 2049
- 1081 Hodges, K. I., 1995: Feature Tracking on the Unit Sphere. *Monthly Weather Review* **123**,  
1082 3458-3465
- 1083 Hodges, K. I., 1996: Spherical Nonparametric Estimators Applied to the UGAMP Model  
1084 Integration for AMIP. *Monthly Weather Review* **124**, 2914-2932
- 1085 Hodges, K. I., 1999: Adaptive Constraints for Feature Tracking. *Monthly Weather Review*  
1086 **127**, 1362-1373
- 1087 Hodges, K. I., A. Cobb, and P. L. Vidale, 2017: How Well Are Tropical Cyclones  
1088 Represented in Reanalysis Datasets? *Journal of Climate* **30**, 5243-5264
- 1089 Hoskins, B. J., and K. I. Hodges, 2019: The Annual Cycle of Northern Hemisphere Storm  
1090 Tracks. Part I: Seasons. *Journal of Climate* **32**, 1743-1760
- 1091 Hoskins, B. J., and P. J. Valdes, 1990: On the Existence of Storm-Tracks. *Journal of the*  
1092 *Atmospheric Sciences* **47**, 1854-1864
- 1093 Ito, R., T. Takemi, and O. Arakawa, 2016: A Possible Reduction in the Severity of Typhoon  
1094 Wind in the Northern Part of Japan under Global Warming: A Case Study. *SOLA* **12**, 100-105

1095 Jones, S. C., P. A. Harr, J. Abraham, L. F. Bosart, P. J. Bowyer, J. L. Evans, D. E. Hanley, B.  
 1096 N. Hanstrum, R. E. Hart, F. Lalaurette, M. R. Sinclair, R. K. Smith, and C. Thorncroft, 2003:  
 1097 The Extratropical Transition of Tropical Cyclones: Forecast Challenges, Current  
 1098 Understanding, and Future Directions. *Weather and Forecasting* **18**, 1052-1092

1099 Judt, F., D. Klocke, R. Rios-Berrios, B. Vanni re, F. Ziemer, L. Auger, J. Biercamp, C.  
 1100 Bretherton, X. Chen, P. D ben, C. Hohenegger, M. Khairoutdinov, C. Kodama, L.  
 1101 Kornbluh, S.-J. Lin, M. Nakano, P. Neumann, W. Putman, N. R ber, M. Roberts, M. Satoh,  
 1102 R. Shibuya, B. Stevens, P. L. Vidale, N. Wedi, and L. Zhou, 2021: Tropical Cyclones in  
 1103 Global Storm-Resolving Models. *Journal of the Meteorological Society of Japan. Ser. II* **99**,  
 1104 579-602

1105 Jung, C., and G. M. Lackmann, 2021: The Response of Extratropical Transition of Tropical  
 1106 Cyclones to Climate Change: Quasi-Idealized Numerical Experiments. *Journal of Climate*  
 1107 **34**, 4361-4381

1108 Keller, J. H., C. M. Grams, M. Riemer, H. M. Archambault, L. Bosart, J. D. Doyle, J. L.  
 1109 Evans, T. J. G. Jr., K. Griffin, P. A. Harr, N. Kitabatake, R. McTaggart-Cowan, F. Pantillon,  
 1110 J. F. Quinting, C. A. Reynolds, E. A. Ritchie, R. D. Torn, and F. Zhang, 2019: The  
 1111 Extratropical Transition of Tropical Cyclones. Part II: Interaction with the Midlatitude Flow,  
 1112 Downstream Impacts, and Implications for Predictability. *Monthly Weather Review* **147**,  
 1113 1077-1106

1114 Kitabatake, N., 2011: Climatology of Extratropical Transition of Tropical Cyclones in the  
 1115 Western North Pacific Defined by Using Cyclone Phase Space. *Journal of the*  
 1116 *Meteorological Society of Japan. Ser. II* **89**, 309-325

1117 Klaver, R., R. Haarsma, P. L. Vidale, and W. Hazeleger, 2020: Effective resolution in high  
 1118 resolution global atmospheric models for climate studies. *Atmospheric Science Letters* **21**,  
 1119 e952

1120 Klein, P. M., P. A. Harr, and R. L. Elsberry, 2002: Extratropical Transition of Western North  
 1121 Pacific Tropical Cyclones: Midlatitude and Tropical Cyclone Contributions to  
 1122 Reintensification. *Monthly Weather Review* **130**, 2240-2259

- 1123 Knutson, T., S. J. Camargo, J. C. L. Chan, K. Emanuel, C.-H. Ho, J. Kossin, M. Mohapatra,  
1124 M. Satoh, M. Sugi, K. Walsh, and L. Wu, 2020: Tropical Cyclones and Climate Change  
1125 Assessment: Part II: Projected Response to Anthropogenic Warming. *Bulletin of the*  
1126 *American Meteorological Society* **101**, E303-E322
- 1127 Kobayashi, S., Y. Ota, Y. Harada, A. Ebita, M. Moriya, H. Onoda, K. Onogi, H. Kamahori,  
1128 C. Kobayashi, H. Endo, K. Miyaoka, and K. Takahashi, 2015: The JRA-55 Reanalysis:  
1129 General Specifications and Basic Characteristics. *Journal of the Meteorological Society of*  
1130 *Japan. Ser. II* **93**, 5-48
- 1131 Kofron, D. E., E. A. Ritchie, and J. S. Tyo, 2010: Determination of a Consistent Time for the  
1132 Extratropical Transition of Tropical Cyclones. Part I: Examination of Existing Methods for  
1133 Finding “ET Time”. *Monthly Weather Review* **138**, 4328-4343
- 1134 Kossin, J. P., K. R. Knapp, D. J. Vimont, R. J. Murnane, and B. A. Harper, 2007: A globally  
1135 consistent reanalysis of hurricane variability and trends. *Geophysical Research Letters* **34**
- 1136 Lanzante, J. R., 2019: Uncertainties in tropical-cyclone translation speed. *Nature* **570**, E6-  
1137 E15
- 1138 Laurila, T. K., V. A. Sinclair, and H. Gregow, 2019: The Extratropical Transition of  
1139 Hurricane Debby (1982) and the Subsequent Development of an Intense Windstorm over  
1140 Finland. *Monthly Weather Review* **148**, 377-401
- 1141 Liu, M., G. A. Vecchi, J. A. Smith, and H. Murakami, 2017: The Present-Day Simulation and  
1142 Twenty-First-Century Projection of the Climatology of Extratropical Transition in the North  
1143 Atlantic. *Journal of Climate* **30**, 2739-2756
- 1144 Liu, M., G. A. Vecchi, J. A. Smith, H. Murakami, R. Gudgel, and X. Yang, 2018: Towards  
1145 Dynamical Seasonal Forecast of Extratropical Transition in the North Atlantic. *Geophysical*  
1146 *Research Letters* **45**, 12,602-612,609
- 1147 Lu, J., G. A. Vecchi, and T. Reichler, 2007: Expansion of the Hadley cell under global  
1148 warming. *Geophysical Research Letters* **34**

- 1149 Manganello, J. V., B. A. Cash, K. I. Hodges, and J. L. Kinter, 2019: Seasonal forecasts of  
1150 North Atlantic tropical cyclone activity in the North American Multi-Model Ensemble.  
1151 *Climate Dynamics* **53**, 7169-7184
- 1152 Michaelis, A. C., and G. M. Lackmann, 2019: Climatological Changes in the Extratropical  
1153 Transition of Tropical Cyclones in High-Resolution Global Simulations. *Journal of Climate*  
1154 **32**, 8733-8753
- 1155 Michaelis, A. C., and G. M. Lackmann, 2021: Storm-Scale Dynamical Changes of  
1156 Extratropical Transition Events in Present-Day and Future High-Resolution Global  
1157 Simulations. *Journal of Climate* **34**, 5037-5062
- 1158 Molod, A., L. Takacs, M. Suarez, and J. Bacmeister, 2015: Development of the GEOS-5  
1159 atmospheric general circulation model: evolution from MERRA to MERRA2. *Geosci. Model*  
1160 *Dev.* **8**, 1339-1356
- 1161 Moon, I.-J., S.-H. Kim, and J. C. L. Chan, 2019: Climate change and tropical cyclone trend.  
1162 *Nature* **570**, E3-E5
- 1163 Moreno-Chamarro, E., L. P. Caron, S. Loosveldt Tomas, J. Vegas-Regidor, O. Gutjahr, M. P.  
1164 Moine, D. Putrasahan, C. D. Roberts, M. J. Roberts, R. Senan, L. Terray, E. Tourigny, and P.  
1165 L. Vidale, 2022: Impact of increased resolution on long-standing biases in HighResMIP-  
1166 PRIMAVERA climate models. *Geosci. Model Dev.* **15**, 269-289
- 1167 Murakami, H., 2014: Tropical cyclones in reanalysis data sets. *Geophysical Research Letters*  
1168 **41**, 2133-2141
- 1169 Rantanen, M., J. Räisänen, V. A. Sinclair, J. Lento, and H. Järvinen, 2020: The extratropical  
1170 transition of Hurricane Ophelia (2017) as diagnosed with a generalized omega equation and  
1171 vorticity equation. *Tellus A: Dynamic Meteorology and Oceanography* **72**, 1-26
- 1172 Roberts, C. D., R. Senan, F. Molteni, S. Boussetta, M. Mayer, and S. P. E. Keeley, 2018:  
1173 Climate model configurations of the ECMWF Integrated Forecasting System (ECMWF-IFS  
1174 cycle 43r1) for HighResMIP. *Geosci. Model Dev.* **11**, 3681-3712
- 1175 Roberts, M. J., A. Baker, E. W. Blockley, D. Calvert, A. Coward, H. T. Hewitt, L. C.  
1176 Jackson, T. Kuhlbrodt, P. Mathiot, C. D. Roberts, R. Schiemann, J. Seddon, B. Vannière, and

1177 P. L. Vidale, 2019: Description of the resolution hierarchy of the global coupled HadGEM3-  
1178 GC3.1 model as used in CMIP6 HighResMIP experiments. *Geosci. Model Dev.* **12**, 4999-  
1179 5028

1180 Roberts, M. J., J. Camp, J. Seddon, P. L. Vidale, K. Hodges, B. Vanniere, J. Mecking, R.  
1181 Haarsma, A. Bellucci, E. Scoccimarro, L.-P. Caron, F. Chauvin, L. Terray, S. Valcke, M.-P.  
1182 Moine, D. Putrasahan, C. Roberts, R. Senan, C. Zarzycki, and P. Ullrich, 2020a: Impact of  
1183 Model Resolution on Tropical Cyclone Simulation Using the HighResMIP-PRIMAVERA  
1184 Multimodel Ensemble. *Journal of Climate* **33**, 2557-2583

1185 Roberts, M. J., J. Camp, J. Seddon, P. L. Vidale, K. Hodges, B. Vannière, J. Mecking, R.  
1186 Haarsma, A. Bellucci, E. Scoccimarro, L.-P. Caron, F. Chauvin, L. Terray, S. Valcke, M.-P.  
1187 Moine, D. Putrasahan, C. D. Roberts, R. Senan, C. Zarzycki, P. Ullrich, Y. Yamada, R.  
1188 Mizuta, C. Kodama, D. Fu, Q. Zhang, G. Danabasoglu, N. Rosenbloom, H. Wang, and L.  
1189 Wu, 2020b: Projected Future Changes in Tropical Cyclones Using the CMIP6 HighResMIP  
1190 Multimodel Ensemble. *Geophysical Research Letters* **47**, e2020GL088662

1191 Roberts, M. J., P. L. Vidale, M. S. Mizieliński, M.-E. Demory, R. Schiemann, J. Strachan, K.  
1192 Hodges, R. Bell, and J. Camp, 2015: Tropical Cyclones in the UPSCALE Ensemble of High-  
1193 Resolution Global Climate Models. *Journal of Climate* **28**, 574-596

1194 Saha, S., S. Moorthi, X. Wu, J. Wang, S. Nadiga, P. Tripp, D. Behringer, Y.-T. Hou, H.-y.  
1195 Chuang, M. Iredell, M. Ek, J. Meng, R. Yang, M. P. Mendez, H. v. d. Dool, Q. Zhang, W.  
1196 Wang, M. Chen, and E. Becker, 2014: The NCEP Climate Forecast System Version 2.  
1197 *Journal of Climate* **27**, 2185-2208

1198 Sainsbury, E. M., R. K. H. Schiemann, K. I. Hodges, L. C. Shaffrey, A. J. Baker, and K. T.  
1199 Bhatia, 2020: How Important Are Post-Tropical Cyclones for European Windstorm Risk?  
1200 *Geophysical Research Letters* **47**, e2020GL089853

1201 Schreck III, C. J., K. R. Knapp, and J. P. Kossin, 2014: The Impact of Best Track  
1202 Discrepancies on Global Tropical Cyclone Climatologies using IBTrACS. *Monthly Weather*  
1203 *Review* **142**, 3881-3899

1204 Sharmila, S., and K. J. E. Walsh, 2018: Recent poleward shift of tropical cyclone formation  
1205 linked to Hadley cell expansion. *Nature Climate Change* **8**, 730-736

1206 Stewart, S. R., 2018: Hurricane Ophelia (AL172017). *National Hurricane Center Tropical*  
1207 *Cyclone Report*, [www.nhc.noaa.gov/data/tcr/AL172017\\_Ophelia.pdf](http://www.nhc.noaa.gov/data/tcr/AL172017_Ophelia.pdf)

1208 Strachan, J., P. L. Vidale, K. Hodges, M. Roberts, and M.-E. Demory, 2013: Investigating  
1209 Global Tropical Cyclone Activity with a Hierarchy of AGCMs: The Role of Model  
1210 Resolution. *Journal of Climate* **26**, 133-152

1211 Studholme, J., A. V. Fedorov, S. K. Gulev, K. Emanuel, and K. Hodges, 2022: Poleward  
1212 expansion of tropical cyclone latitudes in warming climates. *Nature Geoscience* **15**, 14-28

1213 Studholme, J., and S. Gulev, 2018: Concurrent Changes to Hadley Circulation and the  
1214 Meridional Distribution of Tropical Cyclones. *Journal of Climate* **31**, 4367-4389

1215 Studholme, J., K. I. Hodges, and C. M. Brierley, 2015: Objective determination of the  
1216 extratropical transition of tropical cyclones in the Northern Hemisphere. *Tellus A: Dynamic*  
1217 *Meteorology and Oceanography* **67**, 24474

1218 Vanni re, B., M. Roberts, P. L. Vidale, K. Hodges, M.-E. Demory, L.-P. Caron, E.  
1219 Scoccimarro, L. Terray, and R. Senan, 2020: The Moisture Budget of Tropical Cyclones in  
1220 HighResMIP Models: Large-Scale Environmental Balance and Sensitivity to Horizontal  
1221 Resolution. *Journal of Climate* **33**, 8457-8474

1222 Vecchi, G. A., T. L. Delworth, H. Murakami, S. D. Underwood, A. T. Wittenberg, F. Zeng,  
1223 W. Zhang, J. W. Baldwin, K. T. Bhatia, W. Cooke, J. He, S. B. Kapnick, T. R. Knutson, G.  
1224 Villarini, K. van der Wiel, W. Anderson, V. Balaji, J. H. Chen, K. W. Dixon, R. Gudgel, L.  
1225 M. Harris, L. Jia, N. C. Johnson, S.-J. Lin, M. Liu, C. H. J. Ng, A. Rosati, J. A. Smith, and X.  
1226 Yang, 2019: Tropical cyclone sensitivities to CO2 doubling: roles of atmospheric resolution,  
1227 synoptic variability and background climate changes. *Climate Dynamics* **53**, 5999-6033

1228 Vecchi, G. A., and T. R. Knutson, 2008: On Estimates of Historical North Atlantic Tropical  
1229 Cyclone Activity. *Journal of Climate* **21**, 3580-3600

1230 Vecchi, G. A., and T. R. Knutson, 2011: Estimating Annual Numbers of Atlantic Hurricanes  
1231 Missing from the HURDAT Database (1878–1965) Using Ship Track Density. *Journal of*  
1232 *Climate* **24**, 1736-1746



1233 Velden, C., B. Harper, F. Wells, J. L. Beven, R. Zehr, T. Olander, M. Mayfield, C. C. Guard,  
1234 M. Lander, R. Edson, L. Avila, A. Burton, M. Turk, A. Kikuchi, A. Christian, P. Caroff, and  
1235 P. McCrone, 2006: The Dvorak Tropical Cyclone Intensity Estimation Technique: A  
1236 Satellite-Based Method that Has Endured for over 30 Years. *Bulletin of the American*  
1237 *Meteorological Society* **87**, 1195-1210

1238 Vidale, P. L., K. Hodges, B. Vanni re, P. Davini, M. J. Roberts, K. Strommen, A.  
1239 Weisheimer, E. Plesca, and S. Corti, 2021: Impact of Stochastic Physics and Model  
1240 Resolution on the Simulation of Tropical Cyclones in Climate GCMs. *Journal of Climate* **34**,  
1241 4315-4341

1242 Voldoire, A., D. Saint-Martin, S. S n si, B. Decharme, A. Alias, M. Chevallier, J. Colin, J. F.  
1243 Gu r my, M. Michou, M. P. Moine, P. Nabat, R. Roehrig, D. Salas y M lia, R. S f rian, S.  
1244 Valcke, I. Beau, S. Belamari, S. Berthet, C. Cassou, J. Cattiaux, J. Deshayes, H. Douville, C.  
1245 Eth , L. Franchist guy, O. Geoffroy, C. L vy, G. Madec, Y. Meurdesoif, R. Msadek, A.  
1246 Ribes, E. Sanchez-Gomez, L. Terray, and R. Waldman, 2019: Evaluation of CMIP6 DECK  
1247 Experiments With CNRM-CM6-1. *Journal of Advances in Modeling Earth Systems* **11**, 2177-  
1248 2213

1249 Weinkle, J., C. Landsea, D. Collins, R. Musulin, R. P. Crompton, P. J. Klotzbach, and R.  
1250 Pielke, 2018: Normalized hurricane damage in the continental United States 1900–2017.  
1251 *Nature Sustainability* **1**, 808-813

1252 Williams, K. D., D. Copsey, E. W. Blockley, A. Bodas-Salcedo, D. Calvert, R. Comer, P.  
1253 Davis, T. Graham, H. T. Hewitt, R. Hill, P. Hyder, S. Ineson, T. C. Johns, A. B. Keen, R. W.  
1254 Lee, A. Megann, S. F. Milton, J. G. L. Rae, M. J. Roberts, A. A. Scaife, R. Schiemann, D.  
1255 Storkey, L. Thorpe, I. G. Watterson, D. N. Walters, A. West, R. A. Wood, T. Woollings, and  
1256 P. K. Xavier, 2018: The Met Office Global Coupled Model 3.0 and 3.1 (GC3.0 and GC3.1)  
1257 Configurations. *Journal of Advances in Modeling Earth Systems* **10**, 357-380

1258 Wood, K. M., and E. A. Ritchie, 2014: A 40-Year Climatology of Extratropical Transition in  
1259 the Eastern North Pacific. *Journal of Climate* **27**, 5999-6015

1260 Zarzycki, C. M., D. R. Thatcher, and C. Jablonowski, 2017: Objective tropical cyclone  
1261 extratropical transition detection in high-resolution reanalysis and climate model data.  
1262 *Journal of Advances in Modeling Earth Systems* **9**, 130-148

1263 Zhu, X., L. Wu, and Q. Wang, 2018: Extratropical Transition and Re-Intensification of  
1264 Typhoon Toraji (2001): Large-Scale Circulations, Structural Characteristics, and Mechanism  
1265 Analysis. *Journal of Ocean University of China* **17**, 461-476  
1266

## Supplementary information

### Extratropical transition of tropical cyclones in a multiresolution ensemble of atmosphere-only and fully coupled global climate models

Alexander J. Baker<sup>1,\*</sup>, Malcolm J. Roberts<sup>2</sup>, Pier Luigi Vidale<sup>1</sup>, Kevin I. Hodges<sup>1</sup>, Jon Seddon<sup>2</sup>, Benoît Vanni re<sup>1</sup>, Rein J. Haarsma<sup>3</sup>, Reinhard Schiemann<sup>1</sup>, Dimitris Kapetanakis<sup>3</sup>, Etienne Tourigny<sup>4</sup>, Katja Lohmann<sup>5</sup>, Christopher D. Roberts<sup>6</sup>, and Laurent Terray<sup>7</sup>

<sup>1</sup> National Centre for Atmospheric Science and Department of Meteorology, University of Reading, Reading, Berkshire, UK

<sup>2</sup> Met Office Hadley Centre, Exeter, Devon, UK

<sup>3</sup> Koninklijk Nederlands Meteorologisch Instituut, De Bilt, The Netherlands

<sup>4</sup> Earth Sciences Department, Barcelona Supercomputing Center, Barcelona, Spain

<sup>5</sup> Max Planck Institut f r Meteorologie, Hamburg, Germany

<sup>6</sup> European Centre for Medium-Range Weather Forecasts (ECMWF), Reading, UK

<sup>7</sup> Climat, Environnement, Couplages et Incertitudes, Centre Europ en de Recherche et de Formation Avanc e en Calcul Scientifique (CERFACS), Toulouse, France

\* alexander.baker@reading.ac.uk

Corresponding author: Dr Alexander J. Baker

National Centre for Atmospheric Science  
Department of Meteorology,  
University of Reading  
Earley Gate, Whiteknights Road, Reading, Berkshire RG6 6ES, UK  
+44 (0) 118 377 762

## **S1. Methodological considerations**

Two important methodological considerations in ET studies are discussed in this section: (i) the cyclone-tracking algorithm and (ii) the sensitivity of ET location to how ET is identified.

### *S1.1 Cyclone-tracking algorithm*

Recent studies of tropical cyclones in reanalyses and simulated by climate models (e.g., Roberts et al., 2020a; Vanni re et al., 2020) compared results obtained using TRACK with TempestExtremes, a sea-level-pressure-based tracking algorithm (Ullrich and Zarzycki, 2017), to show that, broadly, their results are robust to algorithm choice. However, tracks output by TempestExtremes represent only cyclones' warm-core stages, and as such few identified systems undergo ET (Fig. S1). Therefore, supplementary algorithms are required to extend cyclone tracks generated using TempestExtremes into the midlatitudes (e.g., Michaelis and Lackmann, 2019; Zarzycki et al., 2017), but the extent to which results are sensitive to the additional methodological choices necessary in this approach is unclear. In this study, use of TRACK, a vorticity-based algorithm that satisfactorily yields complete cyclone lifecycles based on a single set of identification criteria, is clearly advantageous in our analysis of ET statistics. Once comparable whole-lifecycle tracks, including post-tropical evolution, from multiple, independent algorithms are available, sensitivity analysis should be a research priority.

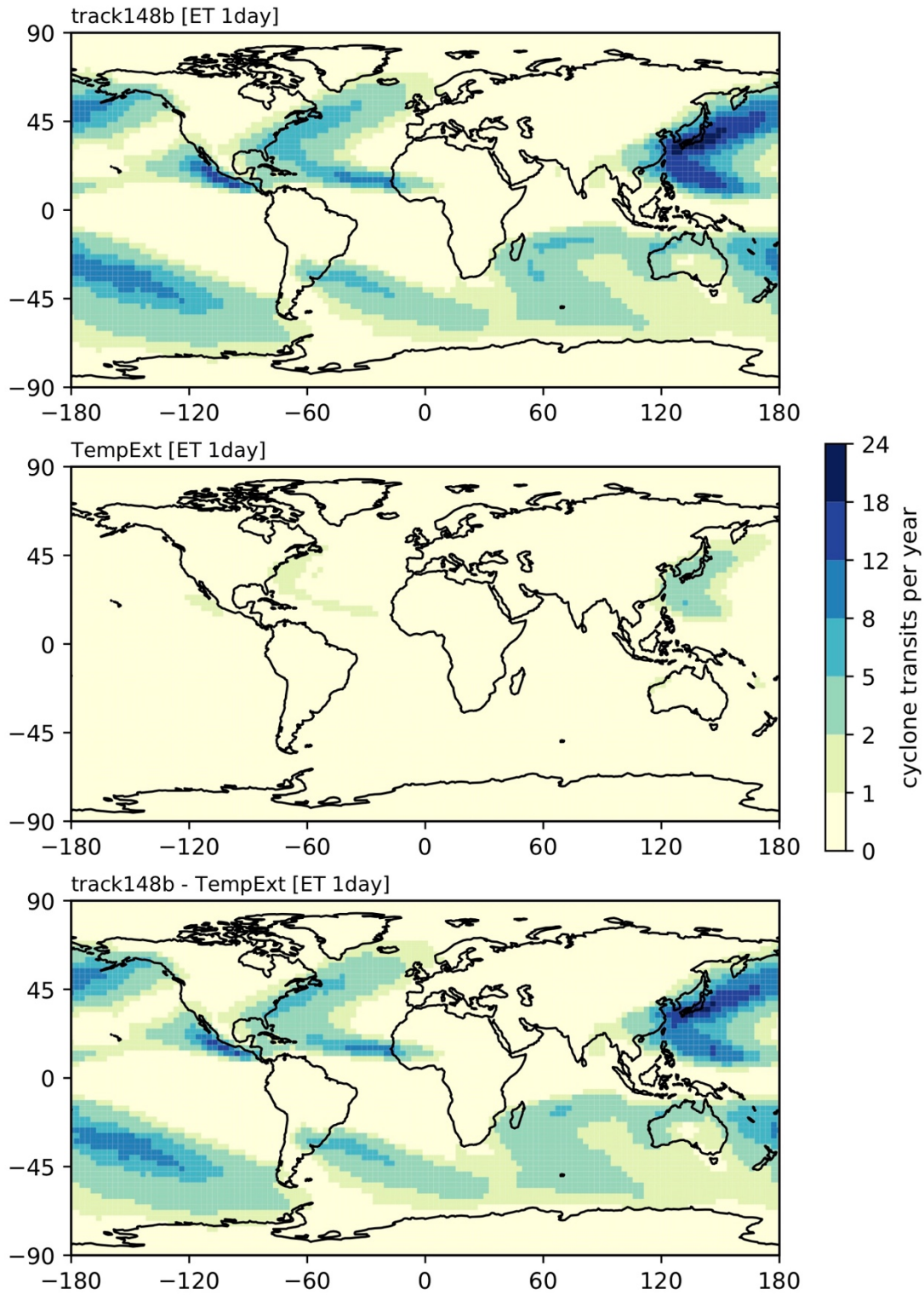


**Fig. S1.** Multi-reanalysis-mean track density in TCs undergoing ET identified by two feature-tracking algorithms: (top) TRACK (“track148b”) and (middle) TempestExtremes (“TempExt”). We also show (bottom) the inter-algorithm difference (i.e., TRACK minus TempestExtremes).

### *S1.2 Sensitivity of ET location to identification method*

Recent analysis of ERA5 shows that phase-space-based identification of post-tropical structures compares well with other methods in terms of the number of ET events identified (Sainsbury et al., 2020) and phase-space methodologies are the most common across studies of ET. However, no consensus approach to identifying ET onset and completion based on phase-space parameters exists. Previous studies have applied differing absolute thresholds to identify changes in cyclone thermal symmetry and employed additional criteria, such as intensity thresholds and temporal smoothing of phase-space series. These modifications have little impact on the number of identified events, but the location of ET may be sensitive to how phase-space parameters are treated. We conducted an overview assessment of this in reanalyses by mapping the mean ET-completion locations for various identification approaches (Fig. S2). In the North Atlantic and Western North Pacific, a definition of ET where both ET onset and completion are identified by single-timestep  $B$  or  $T_L$  changes (‘conventional’) yields the lowest-latitude ET completion (Fig. S2). In contrast, applying a prior warm-core test, as in the previous section (4.2), yields ET completion in the range of 30–40 ° latitude, coinciding with the known centres of baroclinicity associated with western boundary currents. Other proposed modifications of ET identification—imposing a  $v_{max}$  threshold, applying a temporal smoothing, and requiring  $B$  and  $T_L$  criteria are met for consecutive timesteps—yield locations in between these two approaches, with greater overlap seen in the Western North Pacific (Fig. S2). These results help quantify the sensitivity of ET location to various methodological choices, and the results presented in Fig. 16 are necessarily sensitive to such choices, as are other published analyses. The method should fit the research question. When ET completion is identified post-warm core, it is broadly co-located with climatological, basin-high values of Eady growth rate (Fig. S2), indicating that this approach may be preferable for analyses of ET location, particularly in the North Atlantic.

In addition, application to climate models presents additional concerns. Bieli et al. (2020) identified grid-scale convective updrafts in 50-km-resolution simulations with the Forecast-oriented Low Ocean Resolution (FLOR) version of the GFDL CM2.5 that triggered erroneous diagnoses of warm- and cold-core cyclone structures. These were rectified by computing storm-centric 95<sup>th</sup>-percentile geopotential (rather than local maxima) and by applying a temporal smoothing to phase-space trajectories. Although these issues are not pertinent to all models, understanding the effect of convection-parameterisation schemes on geopotential maxima and phase-space results, particularly  $T_U$ , requires a systematic investigation across

multiple high-resolution models, contrasting simulations run using parameterised versus explicitly resolved convection.

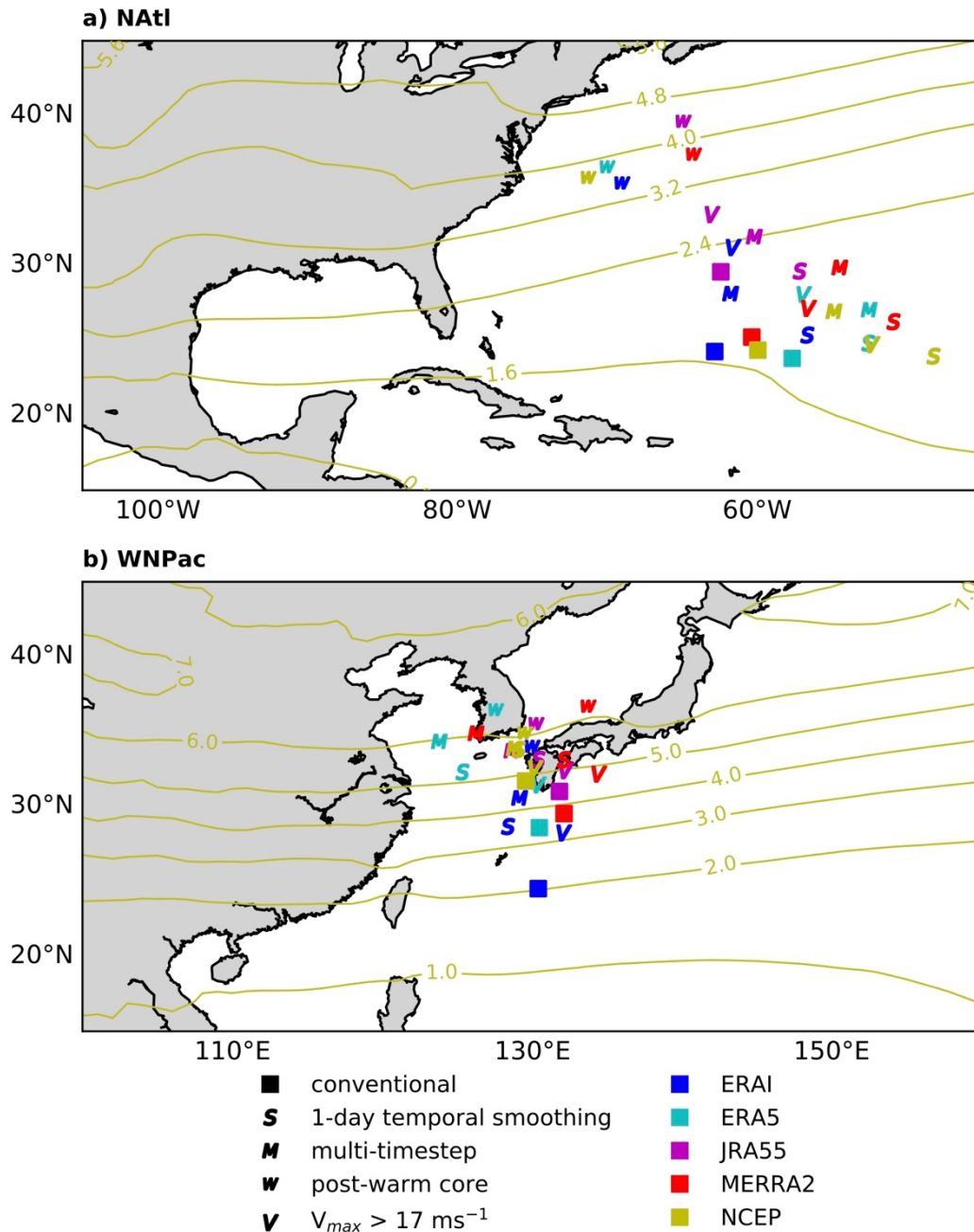


**Fig. S2.** Sensitivity of ET-completion location in reanalyses to published methodological approaches. Results are shown for (a) the North Atlantic ('NAAtl') and (b) the Western North Pacific ('WNPac'). 'Conventional' (square markers) refers to the commonly used definition of ET completion: the first timestep at which both  $B$  and  $T_L$  indicate an extratropical structure. The other markers indicate a single modification of this definition. 'S': a 24-hour temporal smoothing of  $B$  and  $T_L$  trajectories was applied. 'M': ET completion is only identified where  $B$  and  $T_L$  criteria are satisfied for four consecutive timesteps. 'V': ET completion is only

identified for storms whose lifetime-maximum intensity exceeds  $17 \text{ ms}^{-1}$ . ‘WC’: a warm core lasting for at least two days is first identified for each storm and ET completion is identified thereafter. Overlain are contours of climatological-mean Eady growth rate maxima for August–November in units of  $\text{day}^{-1}$ , computed using ERA5 wind and geopotential data using Eq. 4.



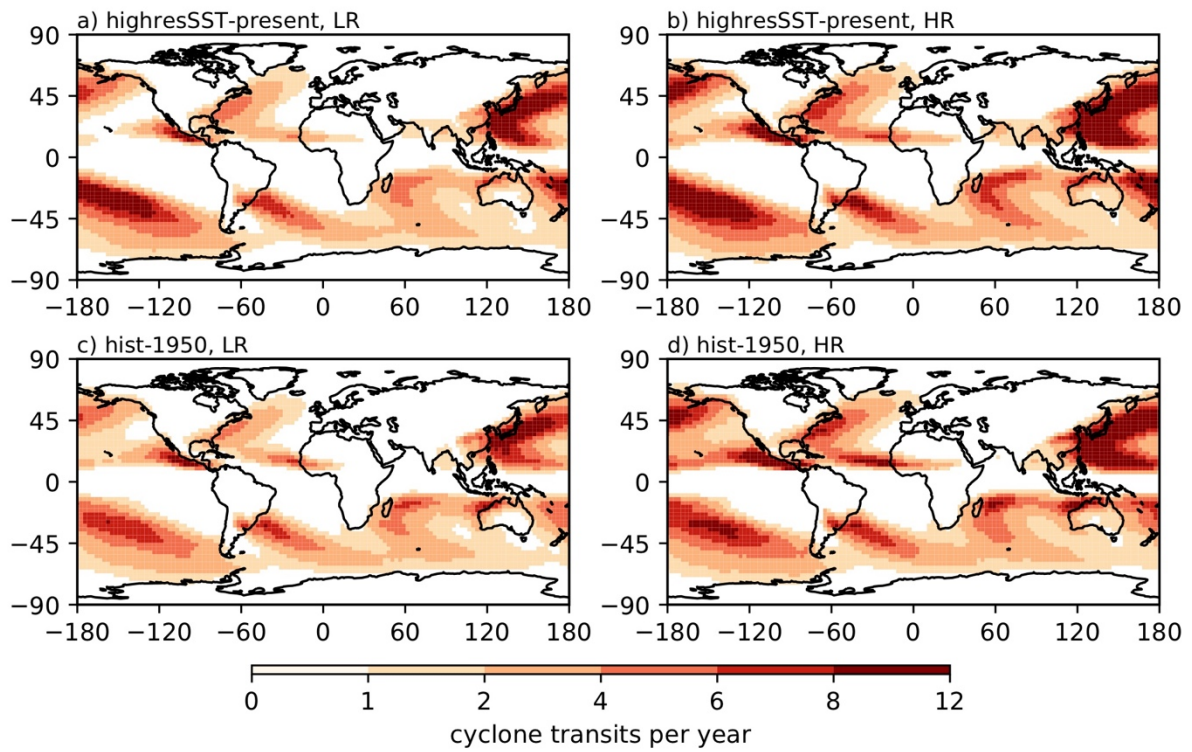


**Fig. S3.** Historical ensemble-mean track density simulated in low- and high-resolution (a–b) *highresSST-present* and (c–d) *hist-1950* experiments. Unit is cyclone transits per year per unit area (within a 5° geodesic radius of storm centres). Colour scale is the same as in Fig. 1a.

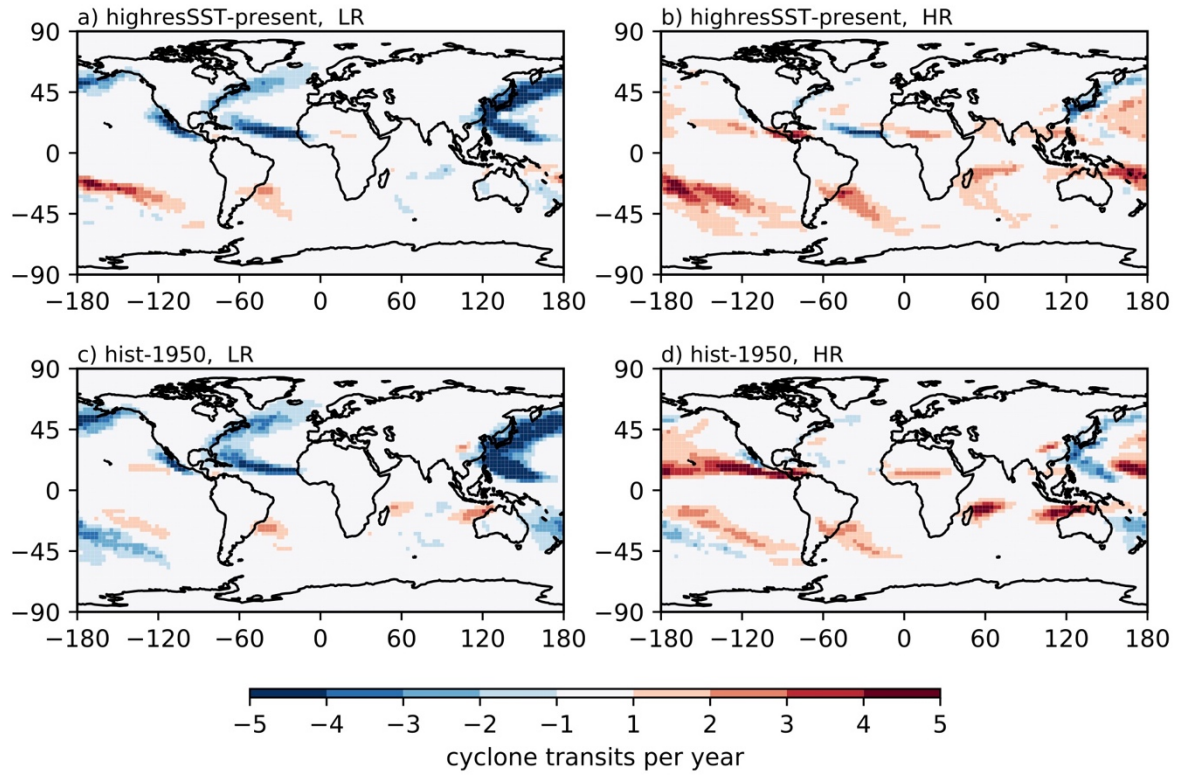


**Fig. S4.** Historical ensemble-mean track density biases (compared with multireanalysis-mean track density) simulated in low- and high-resolution (a–b) *highresSST-present* and (c–d) *hist-1950* experiments. Unit is cyclone transits per year per unit area (within a  $5^\circ$  geodesic radius of storm centres). Colour scale is the same as in Fig. 1c, e.

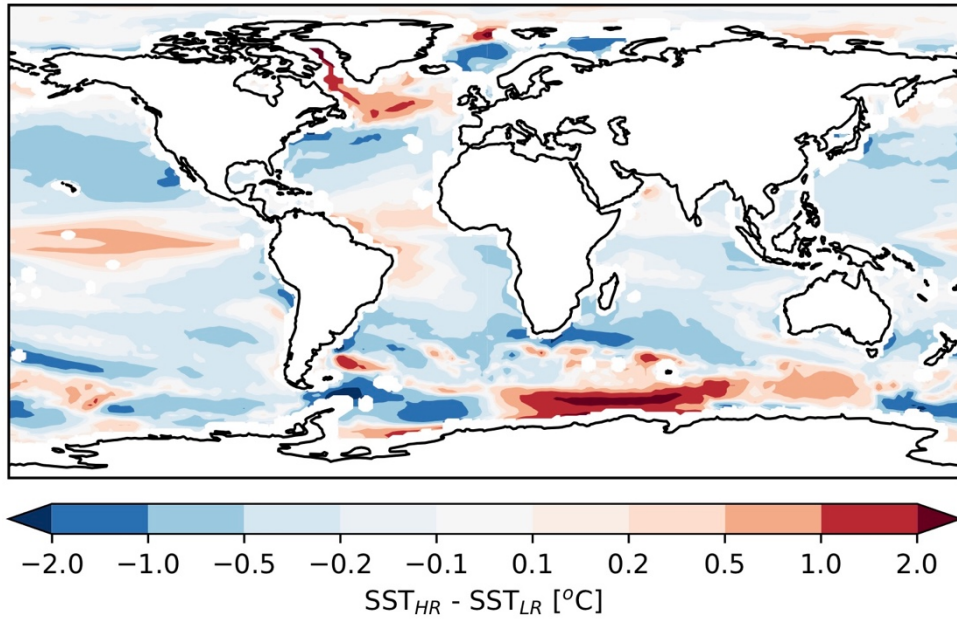


**Fig. S5.** Historical ensemble-mean August-November SST difference between low- and high-resolution *hist-1950* simulations. The low- and high-resolution sub-ensembles correspond to those of Fig. 1. Note the non-linear colour scale.

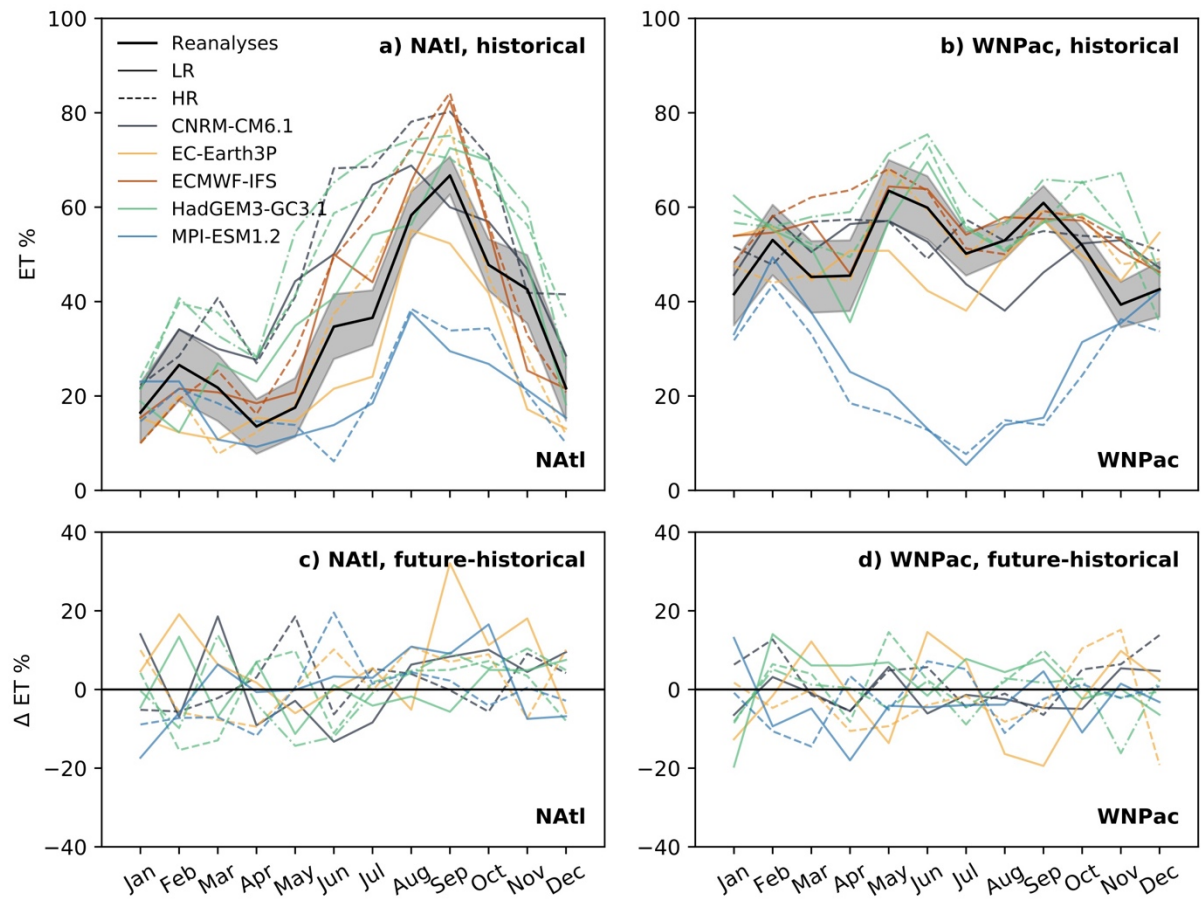


**Fig. S6.** Historical seasonal cycle of ET % in the (a) North Atlantic and (b) Western North Pacific basins. Shown are the multireanalysis mean (black with shading indicating standard error) and low- (solid) and high-resolution (dashed) *highresSST-present* simulations. (c–d) The difference between the future and historical seasonal cycles in ET % (i.e., *highresSST-future* minus *highresSST-present*). HadGEM3-GC3.1-MM is indicated by the dot-dashed line.

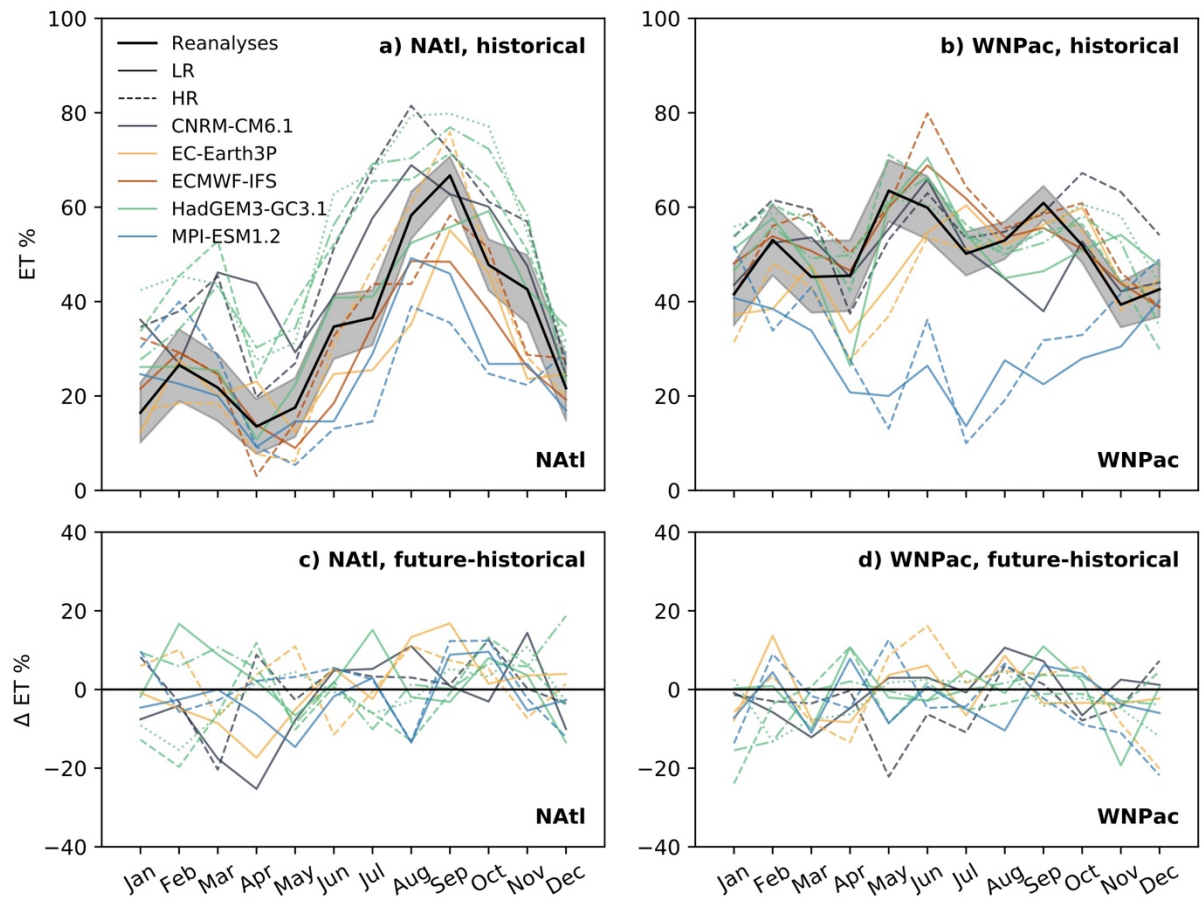


**Fig. S7.** Same as Fig. S6 but for fully coupled simulations. HadGEM3-GC3.1-MM and -HH are indicated by the dot-dashed and dotted lines, respectively.

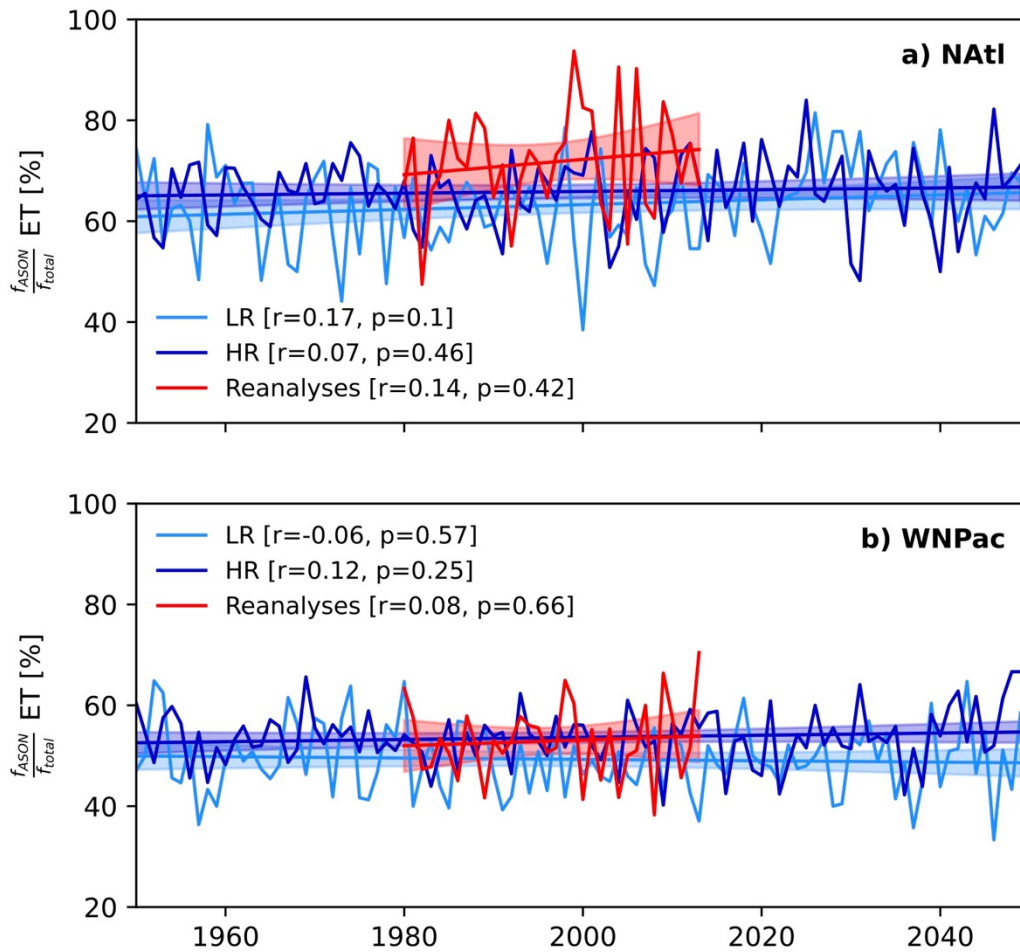


**Fig. S8.** Secular change in the ensemble-mean proportion of ET events occurring during August–November in reanalyses (red) and in low- (pale blue) and high-resolution (dark blue) fully coupled simulations for (a) the North Atlantic and (b) the Western North Pacific basins. Shading shows the 95 % confidence interval for the linear fit. ECMWF-IFS is not included in this analysis because no future simulations were performed in HighResMIP for this model.